Faculty of Fundamental Problems of Technology

DIPLOMA THESIS

Magnetooptical Kerr effect and resonant spin amplification

Kamil Korzekwa

Supervisor: prof. dr hab. inż. Paweł Machnikowski

Wrocław 2012

I would like to thank my supervisor, prof. Paweł Machnikowski, for his friendly guidance, support and wise advices. I would also like to thank dr Tobias Korn and Michael Kugler for helpful discussions and fruitful collaboration. I am grateful for the financial support provided by the TEAM programme of the Foundation for Polish Science co-financed from the European Regional Development Fund.

Contents

Introduction

With its possible applications, including spin memory or semiconductor spin-based quantum computing, spintronics is a very promising branch of nanoscience [1]. However, for the control and readout of spin states one has to maximize their life times. Therefore, a large number of studies of spin dynamics and spin dephasing mechanisms in a vast variety of semiconductors and their heterostructures were performed in recent years [2]. Extended life times observed recently in semiconductor nanostructures (especially for the hole states [3]) seem very promising. Thus, the understanding of the properties of spins in confined semiconductor systems is crucial for the further development and applications of spintronics.

Optical experiments allow one to trace the evolution of electron and hole spins on picosecond time scales. One of such experiments is the time-resolved Kerr rotation (TRKR) measurement [4], that is, the measurement of the rotation of the polarization plane of a reflected beam induced by the spin polarization excited with an earlier pulse. Such an experiment reveals the spin evolution (precession and decoherence) in between the two pulses. If the spin coherence times are comparable with the repetition period of the pulsed laser then a resonant spin amplification (RSA) becomes possible: if the precession frequency is a multiple of the laser repetition period a non-zero spin polarization is established in the system [5].

This work is devoted to theoretical modelling of the TRKR and RSA experiments performed on the p-doped quantum wells (QWs). First, the spin dynamics of the system, induced by optical pumping, is studied. The description of precession in magnetic field, decoherence and recombination processes for various experimental conditions is given. Then, the relation between the studied spin orientation and the measured signal, i.e., experimentally accesible optical field, is constituted. This way the analytical expressions, connecting the spin dynamics and the experimentally measured TRKR and RSA signals, are obtained. These are then used to fit the experimental data and extract spin dynamics parameters of the system. Additionaly, the microscopic spin decoherence mechanism, based on the scattering of thermally released holes on localized ones, is proposed and studied.

Motivation

Although a lot of research has been done concerning the spin dynamics of conduction-band electrons [2, 6] much less attention has been paid to the hole spin dynamics in these systems. This contrast can be explained by the strong spin-orbit coupling within the p-like valence bands in bulk semiconductors, that results in subpicosecond spin dephasing times (SDTs) [7, 8], which is crucial for the control and readout of spin states. However, in p-doped GaAs QWs, in which localization of holes occurs at low temperatures, significantly longer hole SDTs have been observed recently [3, 9, 10]. What is more, due to the p-like wavefunctions of the localized hole states, the contact hyperfine interaction is supressed [11]. Therefore, localized hole states may be more suitable than electron ones for the future applications. Additionally, due to the large anisotropy of the hole g-factor in GaAs-based nanostructures [12], the hole spin dynamics is strongly affected by tilted magnetic fields. This opens the way for spin manipulation schemes based on electrical g-factor control [13, 14].

The purpose and methodology of the thesis

The main purpose of this work is to obtain analytical expressions for the Kerr and RSA optical responses, that can reproduce experimental data for various experimental conditions (like high power or off-resonant pumping). This allows one to extract the spin dynamics parameters of the system, like the intrinsic (homogeneous) spin coherence time T_2, and the g-factor distribution in the ensemble. In order to achieve this the Markovian master equation for the density matrix of the independent hole-trion systems is used, with the decoherence processes described by the universal Lindblad superoperator. The dipole approximation of the light-matter interaction is assumed and the influence of the pump pulse on the system is treated perturbatively. The additional goal is to propose the microscopic model of the spin decoherence that would, at least qualitatively, explain the thermal dependence of the hole spin lifetimes in the p-doped QW. Here, the spin-exchanging scattering probabilities of thermally released holes on localized ones are calculated with the use of Fermi's Golden Rule.

The scope of this work

This thesis is the result of the *Characterization of spin stability, coherence and dephasing by optical experiments* project realized in between 2010 and 2012 as a part of *Semiconductor nanostructures for renewable energy, information processing and communication technologies* research project within the TEAM programme of Foundation for Polish Science. Thanks to the fruitful collaboration with the Optical Spectroscopy of Semiconduc-

tor Quantum Structures experimental group from the Institut für Experimentelle und Angewandte Physik, Universität Regensburg (which will be reffered to as the Regensburg group), the developed theoretical model could be tested by comparison with the real experimental data. That is why, although the author of this thesis is responsible only for the theoretical part, some experimental data are also shown throughout this work. The main reason for this is to fully present the results of the whole project (some of which have already been published, see Ref. [15]) and to prove that, indeed, the proposed theoretical model describes the physical reality correctly.

Theoretical modelling of spin dynamics presented in this work is strongly based on Ref. [16]. Original work consists of three main parts. First, the already existing model was extended to account for the description of spin dynamics in weak magnetic fields (no rotating wave approximation) and for nonresonant excitation (inclusion of the fast hole spin decoherence). Secondly, the description of the resonant spin amplification experiment was elaborated. Finally, the microscopic model of spin decoherence was developed.

Composition of the thesis

The thesis is divided into four chapters. The first chapter contains general description of the investigated system and modeled experiments. In the second one, the Markovian model of the spin dynamics in p-doped QWs is presented. Also the influence of the pump pulse on the system is described, as well as the dependence of the probe pulse linear polarization rotation on the spin orientation at the time it arrives at the sample surface. The third chapter is devoted to the already mentioned microscopic decoherence mechanism and calculation of the spin lifetime dependence on the temperature. In the fourth chapter, all the results are collected. These contain the modelled results for the TRKR and RSA signals for different magnetic field configurations (no magnetic field, Voigt configuration and tilted field) and various excitation conditions (resonant, off-resonant and high power pumping), as well as the fittings to the experimental data and the extracted spin dynamics parameters. The comparison between temperature dependence of spin lifetimes obtained from the microscopic model and the experiment is also presented. Additionaly, at the end of the thesis, appendix devoted to the mathematical formulation of quantum open systems, is attached.

Chapter 1

System and modeled experiments

In this chapter, the physical system, spin dynamics of which is studied in this work, is introduced. The basic facts about the system are presented, as well as the characteristics of the QW sample used in the experiments performed by the Regenburg group. The chapter also contains the general description of the experiments that give insight into the microscopic evolution of the spin polarization, i.e., time resolved Kerr rotation and resonant spin amplification.

1.1 Investigated system

This work focuses on modelling the spin dynamics of the carriers in p-doped semiconductor quantum wells. In such systems, a rapid increase of hole spin dephasing is experimentally observed above a certain threshold temperature. This is associated with thermal release of the carriers from localization centers and the onset of spin-orbit-related dephasing characteristic of free carriers. For applications, however, long spin lifetimes are necessary. Therefore, the focus is put on the low temperature case, when the resident holes are weakly trapped, most likely on QW width fluctuations [3, 14]. Then, the investigated system is composed of localized holes that may be considered as independent and noninteracting. It was also experimentally showed that in such structures at low densities and liquid-helium temperatures, the optical recombination spectra are governed by recombinations of neutral and positively charged excitons (positive trions). The scheme of the investigated system is presented in Fig. 1.1, together with the basis of the Hilbert space, to which the theoretical description is restricted (for more details see Sec. 2.1). It is worth noting that, due to similiar behaviour of localized holes in QW and holes in the ensemble of quantum dots (QDs) in a remotely p-doped structure, the developed theoretical model can also be used in the latter case.

The sample used during the experiments performed by the Regensburg group was

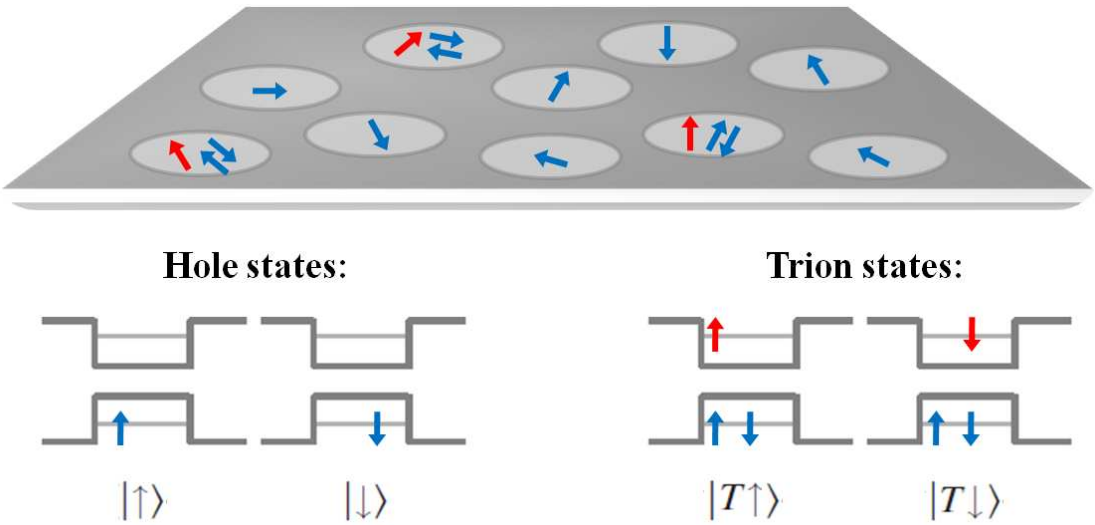

Figure 1.1: Schematic picture of the investigated system (top): the QW with localized hole and electron spins represented by blue and red arrows, respectively. The basis of the considered Hilbert space (bottom): "spin-up" and "spin-down" states with definite projections on the growth axis (normal to the QW plane) for holes ($|\uparrow\rangle$, $|\downarrow\rangle$) and trions ($|T\uparrow\rangle$, $|T\downarrow\rangle$).

a single-side p-modulation-doped GaAs/$Al_{0.3}Ga_{0.7}As$ QW. It had a width of 4 nm and contained two-dimensional hole system with a hole density $p = 1.1 \cdot 10^{11}$ cm^{-2} and mobility $\mu = 1.3 \cdot 10^4$ cm^2/Vs (measured at 1.3 K). It was grown by molecular beam epitaxy from a single wafer.

1.2 Time resolved Kerr rotation

Time resolved Kerr rotation (TRKR) is one of the main experiments used in the study of spin dynamics in nanostructures. It allows one to optically create spin polarization in the system and then to measure the remaining magnetization after some adjustable delay time. The main feature of the TRKR experiment is the pump-probe measuring scheme (Fig. 1.2). First, at a time t_0, a circurarly polarized pump pulse arrives at normal incidence to the sample surface and, due to optical selection rules, creates optically oriented electron-hole pairs. The laser is tuned to the heavy hole transition and is spectrally narrow enough to neglect the light hole contribution due to relatively large heavy-light hole splitting in QWs. This, together with the already mentioned fact about recombination spectra, results in the non-equilibrium heavy hole and positive trion spin polarization in the system (see Fig. 1.3). Then, after the delay time τ, at the time $t_0 + \tau$, a linearly polarized pulse arrives at the structure surface. It induces a time-dependent dipole moment, which

depends on the spin polarization of the system due to different absorption of the left and right circurarly polarized components of the linearly polarized probe pulse. This time-dependent dipole moment is the source of coherent radiation and, together with the reflected part of the probe pulse, is measured in the homodyne detection scheme. The superposition of these two components results in the tilting of the original linear polarization, which is called the Kerr effect (Fig. 1.2). Thus, repeating the experiment with different delay times τ (which is experimentally achieved using a mechanical delay line), one can measure the time evolution of the spin polarization in the system.

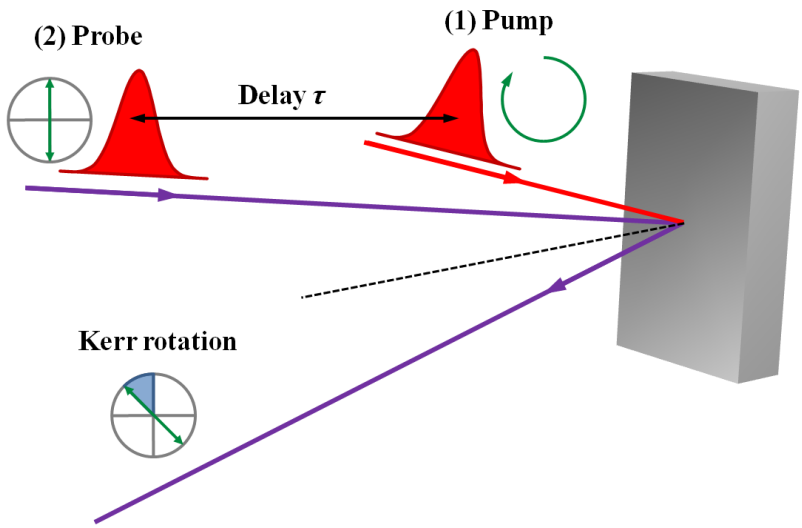

Figure 1.2: Schematic picture of the pump-probe measuring scheme. The Kerr rotation corresponds to the tilt of the original probe pulse linear polarization, after reflection from the spin-polarized surface.

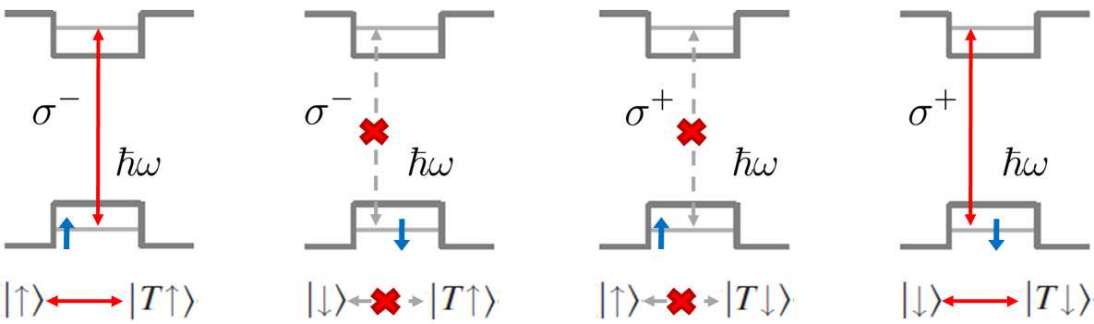

Figure 1.3: Allowed (red, solid lines) and forbidden (grey, dashed lines) transitions in the system for the right and left circurarly polarized excitation.

1.3 Resonant spin amplification

While the TRKR experiment allows one to measure spin dynamics with high temporal resolution, limited only by the precision of the mechanical delay line (usually of the order of a picosecond), it is not the best way to measure long time evolution. This is mainly due to the experimental setup, which needs around 30 cm mechanical delay line for each 1 ns of time evolution. Thus, for measuring long-lived spin dynamics the resonant spin amplification (RSA) technique, with similiar experimental setup, is used. It is based on the interference of spin polarizations created in a sample by subsequent pump pulses. For certain magnitudes of the applied magnetic field, the optically oriented spin polarization precesses around it by an integer multiple of 2π in the time window between subsequent pump pulses, so that constructive interference occurs (the schematic mechanism of formation of the RSA signal is presented in the Fig. 1.4). This is seen in the experiment as pronounced maxima in the Kerr rotation angle measured for a fixed time delay as a function of the applied magnetic field (Fig. 1.5).

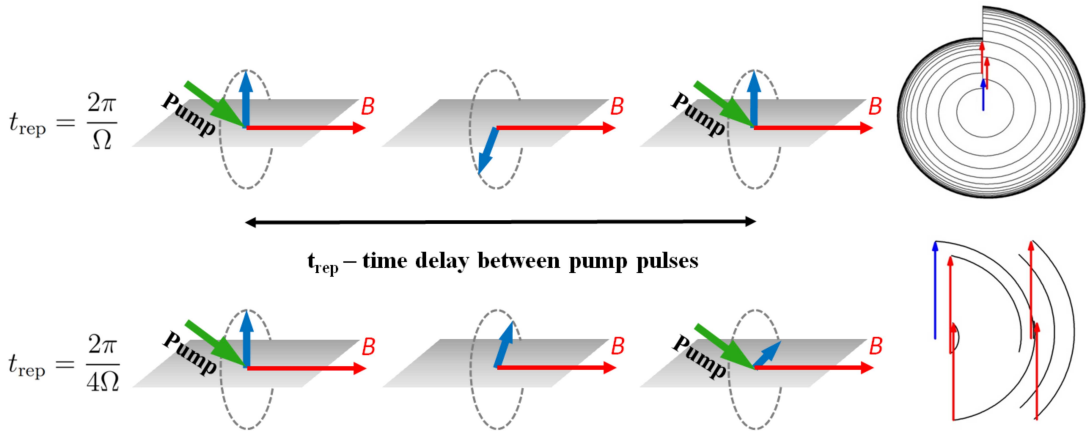

Figure 1.4: Schematic mechanism of formation of the RSA signal. The time delay in between pump pulses (the repetition period), t_{rep}, corresponds to one period of spin precession (top, maximum of constructive interference is obtained) and one quarter of this period (bottom). On the right, the blue arrows represent the spin polarization after the first pump pulse and the red ones show the change of the spin polarization by subsequent pump pulses. The decoherence is included in the picture, so that the spin polarization achieves stable value after some number of pulses.

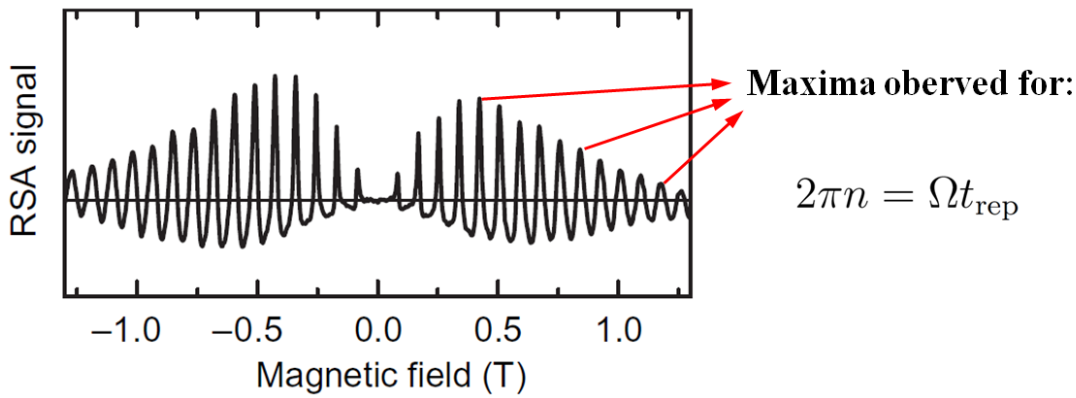

Figure 1.5: Exemplary RSA trace: maxima observed for a magnetic field for which the product of the precession frequency Ω and the repetition period of the pumping laser t_{rep} is an integer multiple of 2π.

Chapter 2

Markovian model of spin dynamics

This chapter contains the detailed information about modelling the spin dynamics in a p-doped QW system in the Markovian limit. Minimal, generic model that is able to account for all the features of the spin dynamics observed in the experiment, without specific assumptions on the detailed mechanism of spin decoherence (which will be described in Chapter 3), is proposed. First, the description of the system in the magnetic field in the density matrix formalism is introduced. Next, the focus is put on the influence of the pump pulse on the system state. This includes two steps: unitary evolution under the excitation tuned to the hole-trion transition and the fast initial hole spin decoherence due to excess energy delivered to the system. Then, the system evolution (Larmor precession, recombination and spin decoherence) is modeled in terms of a Markovian master equation using the universal Lindblad superoperator (more details about this formalism can be found in the Appendix). Next, the descripton of the RSA experiment is given in terms of the repetitive, three-step transformation (pumping, fast decoherence and standard evolution). Finally, the description of the interaction of the probe pulse with the system and the homodyne detection scheme, that results in the Kerr rotation, is given. The derivations and reasoning presented in this chapter are based or inspired by Ref. [16] and [17].

2.1 Model of the investigated system

The optical response of a system composed of localized holes (trapped in QW fluctuations), which will be considered independent (noninteracting), will be modeled. Due to the usually large heavy-light hole splitting in confined systems the description will be restricted only to the heavy hole states, with the assumption that in thermal equilibrium each trapping centre accomadates at most one hole. Taking into account previous experimental findings about the recombination spectra in such systems [3, 14], the fundamental

optical transition at each trapping center is described as an excitation of an electron-hole pair, which, together with the resident hole, forms a bound trion. All these assumptions allow to describe the optical response in terms of independent hole-trion systems. The driving pulse is also assumed to be spectrally narrow and temperature low enough, so that the description of the system can be restricted to the lowest hole and trion states.

The state of such system will be represented by the density matrix ρ, restricted to the four states, $|\uparrow\rangle$, $|\downarrow\rangle$, $|T\uparrow\rangle$, $|T\downarrow\rangle$, that represent the two hole and the two trion states with different spin orientations (with respect to the normal to the QW plane). Now, the density matrix can be parametrized by introducing the set of dynamical variables describing the evolution of the system. These consists of the trion and hole populations,

$$\begin{aligned} N_{\mathrm{t}}(t) &= \mathrm{Tr}\left(\hat{N}_{\mathrm{t}}\rho(t)\right), \quad \hat{N}_{\mathrm{t}} = \tfrac{1}{\sqrt{2}}\left(|T\uparrow\rangle\langle T\uparrow| + |T\downarrow\rangle\langle T\downarrow|\right), \\ N_{\mathrm{h}}(t) &= 1 - N_{\mathrm{t}}(t), \end{aligned} \tag{2.1}$$

the trion and hole spin polarizations,

$$\begin{aligned} \Sigma_{\mathrm{t}}(t) &= \mathrm{Tr}\left(\hat{\Sigma}_{\mathrm{t}}\rho(t)\right), \quad \hat{\Sigma}_{\mathrm{t}} = \tfrac{1}{\sqrt{2}}\left(|T\uparrow\rangle\langle T\uparrow| - |T\downarrow\rangle\langle T\downarrow|\right), \\ \Sigma_{\mathrm{h}}(t) &= \mathrm{Tr}\left(\hat{\Sigma}_{\mathrm{h}}\rho(t)\right), \quad \hat{\Sigma}_{\mathrm{h}} = \tfrac{1}{\sqrt{2}}\left(|\uparrow\rangle\langle\uparrow| - |\downarrow\rangle\langle\downarrow|\right), \end{aligned} \tag{2.2}$$

and the trion and hole spin coherences,

$$\begin{aligned} X_{\mathrm{t}}(t) &= \mathrm{Tr}\left(\hat{X}_{\mathrm{t}}\rho(t)\right), \quad \hat{X}_{\mathrm{t}} = \tfrac{1}{\sqrt{2}}\left(|T\uparrow\rangle\langle T\downarrow| + |T\downarrow\rangle\langle T\uparrow|\right), \\ X_{\mathrm{h}}(t) &= \mathrm{Tr}\left(\hat{X}_{\mathrm{h}}\rho(t)\right), \quad \hat{X}_{\mathrm{h}} = \tfrac{1}{\sqrt{2}}\left(|\uparrow\rangle\langle\downarrow| + |\downarrow\rangle\langle\uparrow|\right), \\ Y_{\mathrm{t}}(t) &= \mathrm{Tr}\left(\hat{Y}_{\mathrm{t}}\rho(t)\right), \quad \hat{Y}_{\mathrm{t}} = \tfrac{1}{\sqrt{2}}\left(-i|T\uparrow\rangle\langle T\downarrow| + i|T\downarrow\rangle\langle T\uparrow|\right), \\ Y_{\mathrm{h}}(t) &= \mathrm{Tr}\left(\hat{Y}_{\mathrm{h}}\rho(t)\right), \quad \hat{Y}_{\mathrm{h}} = \tfrac{1}{\sqrt{2}}\left(-i|\uparrow\rangle\langle\downarrow| + i|\downarrow\rangle\langle\uparrow|\right). \end{aligned} \tag{2.3}$$

In this way, the density matrix describing the system can be represented with variables corresponding to the quantities of interest,

$$\rho(t) = \begin{pmatrix} \frac{1-N_{\mathrm{t}}(t)+\Sigma_{\mathrm{h}}(t)}{2} & \frac{1}{2}X_{\mathrm{h}}(t) - \frac{i}{2}Y_{\mathrm{h}}(t) & 0 & 0 \\ \frac{1}{2}X_{\mathrm{h}}(t) + \frac{i}{2}Y_{\mathrm{h}}(t) & \frac{1-N_{\mathrm{t}}(t)-\Sigma_{\mathrm{h}}(t)}{2} & 0 & 0 \\ 0 & 0 & \frac{N_{\mathrm{t}}(t)+\Sigma_{\mathrm{t}}(t)}{2} & \frac{1}{2}X_{\mathrm{t}}(t) - \frac{i}{2}Y_{\mathrm{t}}(t) \\ 0 & 0 & \frac{1}{2}X_{\mathrm{t}}(t) + \frac{i}{2}Y_{\mathrm{t}}(t) & \frac{N_{\mathrm{t}}(t)-\Sigma_{\mathrm{t}}(t)}{2} \end{pmatrix}.$$

Next, the system is placed in a magnetic field $\boldsymbol{B}$ oriented at an angle θ with respect to the growth axis (see Fig. 2.1). Throughout this work, the system will be described in a reference frame rotating with the zero-field hole-trion transition frequency ω. The Hamiltonian describing a single trapped hole-trion system in the magnetic field is thus given by,

$$H_0 = -\frac{1}{2}\mu_{\mathrm{B}}\boldsymbol{B}\hat{g}_{\mathrm{h}}\boldsymbol{\sigma}_{\mathrm{h}} - \frac{1}{2}g_{\mathrm{t}}\mu_{\mathrm{B}}\boldsymbol{B}\cdot\boldsymbol{\sigma}_{\mathrm{t}}, \tag{2.4}$$

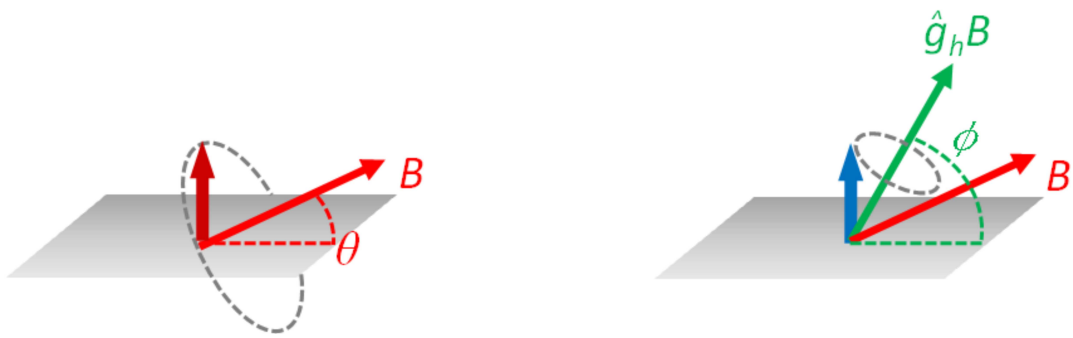

Figure 2.1: Quantization axes for the trion (left) and hole (right) spin.

where μ_B is the Bohr magneton, $\hat{g}_\mathrm{h}$ is the hole Landé tensor, g_t is the Landé factor of the trion (i.e., of the electron), which is assumed to be isotropic, and $\boldsymbol{\sigma}_\mathrm{h}, \boldsymbol{\sigma}_\mathrm{t}$ are the vectors of Pauli matrices corresponding to the hole and trion spin, respectively (the hole is treated as a pseudo-spin-1/2 system). In order to define the Zeeman eigenstates for the magnetically anisotropic hole, its quantization axis has to be found (see Fig. 2.1). The hole Landé tensor is assumed to have no in-plane anisotropy and the magnetic field is set in the xz plane

$$\boldsymbol{B} = B(\sin\theta, 0, \cos\theta) = B\hat{e}_B, \qquad \hat{g}_h = \begin{pmatrix} g_\perp & 0 & 0 \\ 0 & g_\perp & 0 \\ 0 & 0 & g_\parallel \end{pmatrix}.$$

Introducing the effective hole Landé factor $\tilde{g} = (g_\perp^2 \sin^2\theta + g_\parallel^2 \cos^2\theta)^{\frac{1}{2}}$ and the angle ϕ such that $\tan\phi = (g_\perp/g_\parallel)\tan\theta$, the hole spin quantization axis $\hat{e}_\parallel$ can be defined by the equation

$$\hat{e}_B \hat{g}_h = \tilde{g}\left(\frac{g_\perp \sin\theta}{\tilde{g}}, 0, \frac{g_\parallel \cos\theta}{\tilde{g}}\right) = \tilde{g}(\sin\phi, 0, \cos\phi) = \tilde{g}\hat{e}_\parallel. \tag{2.5}$$

This way, the Hamiltonian of the system can be rewritten in the more symmetric form by introducing Pauli matrices coressponding to quantization axes $\sigma_\mathrm{h}^\parallel = \sin\phi\sigma_\mathrm{h}^x + \cos\phi\sigma_\mathrm{h}^z$ and $\sigma_\mathrm{t}^\parallel = \sin\theta\sigma_\mathrm{h}^x + \cos\theta\sigma_\mathrm{t}^z$,

$$H_0 = -\frac{1}{2}\mu_\mathrm{B} B(\tilde{g}\sigma_\mathrm{h}^\parallel + g_\mathrm{t}\sigma_\mathrm{t}^\parallel).$$

Note that in this form, the hole and trion parts of the Hamiltonian differ by the substitution $g_\mathrm{t} \to \tilde{g}$ and $\theta \to \phi$. The last step is to rewrite the Hamiltonian in the basis of its eigenstates, which are actually the eigenstates of the $\sigma_\mathrm{h}^\parallel$ and $\sigma_\mathrm{t}^\parallel$ operators. The eigenvalues $\lambda_{1,2} = \pm 1$ and corresponding eigenstates are found by direct calculation in the form

$$\begin{aligned} |+\rangle &= \cos\tfrac{\phi}{2}|\uparrow\rangle + \sin\tfrac{\phi}{2}|\downarrow\rangle, & |-\rangle &= -\sin\tfrac{\phi}{2}|\uparrow\rangle + \cos\tfrac{\phi}{2}|\downarrow\rangle, \\ |T+\rangle &= \cos\tfrac{\theta}{2}|T\uparrow\rangle + \sin\tfrac{\theta}{2}|T\downarrow\rangle, & |T-\rangle &= -\sin\tfrac{\theta}{2}|T\uparrow\rangle + \cos\tfrac{\theta}{2}|T\downarrow\rangle. \end{aligned}$$

Finally, introducing $\omega_\mathrm{h} = \mu_\mathrm{B} B\tilde{g}/\hbar$ and $\omega_\mathrm{t} = \mu_\mathrm{B} B g_\mathrm{t}/\hbar$, the Hamiltonian takes the form

$$H_0 = \frac{1}{2}\hbar\omega_\mathrm{h}(|-\rangle\langle-| - |+\rangle\langle+|) + \frac{1}{2}\hbar\omega_\mathrm{t}(|T-\rangle\langle T-| - |T+\rangle\langle T+|). \tag{2.6}$$

2.2 Interaction with the pump pulse

At moment $t = 0^-$, just before the arrival of the pump pulse, the system is described by the density matrix ρ_0. The trion dynamical variables in this initial density matrix are equal to 0, which is obvious for the TRKR experiment and justified in the case of RSA experiment by the short lifetimes of trions (time between the pulses in RSA experiment is long enough for carriers to recombine). Thus, at the arrival of the pump pulse, the system is described by

$$\rho_0 = \begin{pmatrix} \frac{1+\Sigma_\mathrm{h}^{(0)}}{2} & \frac{1}{2}X_\mathrm{h}^{(0)} - \frac{i}{2}Y_\mathrm{h}^{(0)} & 0 & 0 \\ \frac{1}{2}X_\mathrm{h}^{(0)} + \frac{i}{2}Y_\mathrm{h}^{(0)} & \frac{1-\Sigma_\mathrm{h}^{(0)}}{2} & 0 & 0 \\ 0 & 0 & 0 & 0 \\ 0 & 0 & 0 & 0 \end{pmatrix}.$$

Initially, spins of the trapped holes are described by thermal equilibrium state, $\rho_0 = \rho_\mathrm{eq}$, which results in the spin polarization along the hole spin quantization axis

$$p = \langle+|\rho_\mathrm{eq}|+\rangle - \langle-|\rho_\mathrm{eq}|-\rangle = \tanh\left(\frac{\hbar\omega_\mathrm{h}}{2k_\mathrm{B}T}\right). \tag{2.7}$$

This is translated into the initial values for the dynamical variables of the holes,

$$\begin{aligned} N_\mathrm{h}^{(0)} &= N_\mathrm{h}^{(\mathrm{eq})} &&= 1, \\ \Sigma_\mathrm{h}^{(0)} &= \Sigma_\mathrm{h}^{(\mathrm{eq})} &&= p\cos\phi, \\ X_\mathrm{h}^{(0)} &= X_\mathrm{h}^{(\mathrm{eq})} &&= p\sin\phi, \\ Y_\mathrm{h}^{(0)} &= Y_\mathrm{h}^{(\mathrm{eq})} &&= 0. \end{aligned} \tag{2.8}$$

Then, at $t = 0$, a circularly polarized pump pulse with frequency $\omega_\mathrm{p} = \omega + \Delta$ (where ω is the hole-trion transition frequency) arrives perpendicularly to the QW plane. To focus attention the pulse is chosen to be circularly right polarized (σ_+),

$$\boldsymbol{\mathcal{E}}(t) = \frac{\boldsymbol{\mathcal{E}}_0}{2}\eta\left(\frac{t}{\tau_\mathrm{p}}\right)e^{-i\omega_\mathrm{p}t+i\psi} + \mathrm{c.c.}, \quad \boldsymbol{\mathcal{E}}_0 = \frac{\mathcal{E}_0}{\sqrt{2}}\begin{pmatrix} 1 \\ i \\ 0 \end{pmatrix},$$

where $\eta(t/\tau_\mathrm{p}) = \exp[-(t/\tau_\mathrm{p})^2/2]$ is the Gaussian pulse shape of length τ_p. The electric field is assumed to couple to the interband transitions via a dipole moment $\boldsymbol{d}$. Then,

in the reference frame rotating with transition frequency ω and using the rotating wave approximation, the interaction Hamiltonian takes the form

$$H_{\mathrm{p}} = \frac{1}{2} f(t) e^{i\Delta t - i\psi} |\uparrow\rangle\langle T\uparrow| + \mathrm{H.c.}, \tag{2.9}$$

where $f(t) = -\boldsymbol{d} \cdot \boldsymbol{\mathcal{E}}_0^*(1+r)\eta(t/\tau_{\mathrm{p}})$ is the envelope function and $r = (1-n)/(1+n)$ is the reflection amplitude at the semiconductor-vacuum interface (n is the refractive index of the capping layer).

Now, assuming that the pulse is much shorter than any relevant time scale of the system dynamics, the change of the system state induced by the pump pulse can be described as instantaneous. The transformation of the initial density matrix ρ_0 into ρ_1 is decribed up to the second order in the pulse amplitude,

$$\rho_1 = -\frac{i}{\hbar} \int_{-\infty}^{\infty} dt \, [H_{\mathrm{p}}(t), \rho_0] - \frac{1}{\hbar^2} \int_{-\infty}^{\infty} dt \int_{-\infty}^{\infty} dt' \, [H_{\mathrm{p}}(t), [H_{\mathrm{p}}(t'), \rho_0]] \, . \tag{2.10}$$

Note that, although for the zero detuning (i.e., $\Delta = 0$) the effect of the pump pulse can be described in an analytical form (which is actually done for the probe pulse, where the detuning is neglected, see Sec. 2.6), in the low power limit the second order perturbative form is a very good approximation and has the advantage of describing also detuned pulses. Now, the transformation induced by the pump pulse can be found by the direct calculation of the commutators.

To shorten the notation and make the result more transparent, the density matrix transformations (this and the following ones, in the next sections) will not be described by writing down all the matrix elements after transformation. Instead, the transformation formulas for the quantities of interest, i.e., N_{h}, Σ_{h}, X_{h}, Y_{h}, N_{t}, Σ_{t}, X_{t}, Y_{t} will be given. Out of these eight variables four can be eliminated. First, recall that $N_{\mathrm{h}} = 1 - N_{\mathrm{t}}$. Secondly, note that during recombination trion variables vanish very quickly, but their initial values (just after the pump pulse) govern the evolution of the hole variables. However, the pump pulse does not transform trion coherences, so throughout the whole evolution they are equal to 0. Finally, the trion population created by the pump pulse is optically oriented, so that $N_{\mathrm{t}} = \Sigma_{\mathrm{t}}$. Thus, the vectors $\boldsymbol{S_0}$ and $\boldsymbol{S_1}$, composed of the important dynamical variables and corresponding to density matrices ρ_0 and ρ_1, can be introduced,

$$\boldsymbol{S}_0 = \boldsymbol{S}^{(\mathrm{eq})} = \begin{pmatrix} \Sigma_{\mathrm{h}}^{(0)} \\ X_{\mathrm{h}}^{(0)} \\ Y_{\mathrm{h}}^{(0)} \\ \Sigma_{\mathrm{t}}^{(0)} \end{pmatrix}, \quad \boldsymbol{S}_1 = \begin{pmatrix} \Sigma_{\mathrm{h}}^{(1)} \\ X_{\mathrm{h}}^{(1)} \\ Y_{\mathrm{h}}^{(1)} \\ \Sigma_{\mathrm{t}}^{(1)} \end{pmatrix} = \hat{A}_{\mathrm{p}} \boldsymbol{S}_0 + \boldsymbol{b}_{\mathrm{p}}.$$

The pump pulse transformation matrix $\hat{A}_\mathrm{p}$ and vector $\boldsymbol{b}_\mathrm{p}$ are given by

$$\hat{A}_\mathrm{p} = \begin{pmatrix} 1-2|F(\Delta)|^2 & 0 & 0 & 0 \\ 0 & 1-2|F(\Delta)|^2 & -2M(\Delta) & 0 \\ 0 & 2M(\Delta) & 1-2|F(\Delta)|^2 & 0 \\ 2|F(\Delta)|^2 & 0 & 0 & 0 \end{pmatrix}, \tag{2.11}$$

$$\boldsymbol{b}_\mathrm{p} = \begin{pmatrix} -2|F(\Delta)|^2 \\ 0 \\ 0 \\ 2|F(\Delta)|^2 \end{pmatrix}, \tag{2.12}$$

where

$$F(\Delta) = \frac{1}{4\hbar}\int_{-\infty}^{\infty} f(t)e^{-i\Delta t}dt = \frac{\hat{f}(\Delta)}{4\hbar},$$
$$M(\Delta) = \frac{1}{16\pi\hbar^2}\mathcal{P}\int_{-\infty}^{\infty}\frac{\hat{f}(\omega)\hat{f}(-\omega)}{\omega+\Delta}d\omega,$$

and $\hat{f}$ is the Fourier transform of the envelope function. Note that for zero detuning, $M(0) = 0$ and $F(0)$ is straightforwardly connected to the area of the pump pulse.

2.3 Initial fast decoherence

For the off-resonant or high power pumping, some amount of excess energy is delivered to the system. In this case, the microscopic kinetics of the system may be quite complex. For example, for the off-resonant excitation, hole spin flips during relaxation to low-energy states are possible, which is clearly beyond the four-level model introduced here. However, the essential effect is bringing the hole spin polarization toward equilibrium and dephasing of the hole spin coherence. Both these effects are included in the model in terms of a fast partial decoherence (relaxation and dephasing) of the hole spins, with the assumption that it takes place on time scales much shorter than the subsequent spin dynamics and can thus be modeled as instantaneous. Taking into account the fast character of the process (comparing to the Larmor precession), the effects of occupation relaxation and additional pure dephasing are associated with the system symmetry axis (coinciding with the axis of optical orientation). Therefore, the matrix elements of density matrix ρ_2, describing the system after the fast decoherence, are connected with the matrix elements of ρ_1, with the use of factors e^{-u} and e^{-w} (responsible for the occupation relaxation and pure dephasing,

respectively),

$$\begin{aligned}
\langle\downarrow|\rho_2|\uparrow\rangle &= \langle\downarrow|\rho_1|\uparrow\rangle e^{-u/2-w}, \\
\langle\uparrow|\rho_2|\downarrow\rangle &= \langle\uparrow|\rho_1|\downarrow\rangle e^{-u/2-w}, \\
\langle\uparrow|\rho_2|\uparrow\rangle &= \tfrac{1}{2}\langle\uparrow|\rho_1|\uparrow\rangle\left(1+e^{-u}\right)+\tfrac{1}{2}\langle\downarrow|\rho_1|\downarrow\rangle\left(1-e^{-u}\right), \\
\langle\downarrow|\rho_2|\downarrow\rangle &= \tfrac{1}{2}\langle\downarrow|\rho_1|\downarrow\rangle\left(1-e^{-u}\right)+\tfrac{1}{2}\langle\downarrow|\rho_1|\downarrow\rangle\left(1+e^{-u}\right).
\end{aligned} \tag{2.13}$$

Again, this process can be described in terms of a transformation of the already introduced vectors $\boldsymbol{S_1}$ and $\boldsymbol{S_2}$, representing the density matrices ρ_1 and ρ_2, respectively,

$$\begin{aligned}
\boldsymbol{S}_2 &= \begin{pmatrix} \Sigma_{\mathrm{h}}^{(2)} \\ X_{\mathrm{h}}^{(2)} \\ Y_{\mathrm{h}}^{(2)} \\ \Sigma_{\mathrm{t}}^{(2)} \end{pmatrix} = \hat{A}_{\mathrm{fd}}\left(\boldsymbol{S}_1-\boldsymbol{S}^{(\mathrm{eq})}\right)+\boldsymbol{S}^{(\mathrm{eq})}, \\
\hat{A}_{\mathrm{fd}} &= \begin{pmatrix} e^{-u} & 0 & 0 & 0 \\ 0 & e^{-u/2-w} & 0 & 0 \\ 0 & 0 & e^{-u/2-w} & 0 \\ 0 & 0 & 0 & 1 \end{pmatrix},
\end{aligned} \tag{2.14}$$

where the $\boldsymbol{S}^{(\mathrm{eq})}$ terms assure that the fast decoherence brings the dynamical variables to the equilibrium, not 0, values.

2.4 Precession, decoherence and recombination

The next step is to model the actual spin dynamics (i.e., Larmor precession, recombination and spin decoherence) in between the pump and probe pulses. In order to achieve this, a Markovian master equation (again, in the rotating frame with respect to the interband transition energy, but in the Schrödinger picture with respect to the spin dynamics) is used [see Eq. (A.12)],

$$\dot{\rho} = -\frac{i}{\hbar}[H_0,\rho]+\mathcal{L}_{\mathrm{h}}[\rho]+\mathcal{L}_{\mathrm{t}}[\rho]+\mathcal{L}_{\mathrm{r}}[\rho], \tag{2.15}$$

where H_0 is given by Eq. (2.6) and, due to the description in Markov limit (which is reasonable in view of the relatively long time scales involved), the dissipative dynamics (decoherence and recombination) is described by the universal Lindblad superoperator $\mathcal{L}=\mathcal{L}_{\mathrm{h}}+\mathcal{L}_{\mathrm{t}}+\mathcal{L}_{\mathrm{r}}$. In the Appendix, the general Lindblad equation for arbitrary dimension of the system Hilbert space is derived. Here, these results are used to find the expressions corresponding to the dissipative dynamics of the considered system, i.e., for the hole dissipator $\mathcal{L}_{\mathrm{h}}$, the trion dissipator $\mathcal{L}_{\mathrm{t}}$ and the spontaneous emission generator $\mathcal{L}_{\mathrm{r}}$.

First, the description of the hole and trion dissipators will be given. Apart from the assumptions given in the Appendix (i.e., Markovian approximation), it is also assumed

that the reservoirs coupled to electron (trion) and hole spins are uncorrelated. Thus, the problem splits into two independent, two-level systems coupled to the environment. The description of the dissipative dynamics of the two systems will be therefore identical, so only the hole case will be discussed and the trion one can be obtained after substitutions: $\phi \to \theta$, $\omega_{\mathrm{h}} \to \omega_{\mathrm{t}}$, $|\uparrow\rangle \to |T\uparrow\rangle$ and $|\downarrow\rangle \to |T\downarrow\rangle$.

Following the derivation from the Appendix (here the double index of the σ operators is omitted, since for a two-level system only 3 operators are required), the spin-environment interaction Hamiltonian can be written as [see Eq. (A.6)]

$$H_{\mathrm{int}} = \sum_i \sigma_i^{(\mathrm{h})} R_i^{(\mathrm{h})} = \sigma_x^{(\mathrm{h})} R_x^{(\mathrm{h})} + \sigma_y^{(\mathrm{h})} R_y^{(\mathrm{h})} + \sigma_z^{(\mathrm{h})} R_z^{(\mathrm{h})}, \tag{2.16}$$

where $\sigma_i^{(\mathrm{h})}$ are the Pauli matrices and $R_i^{(\mathrm{h})}$ are certain operators on the Hilbert space of the reservoir. However, to use the open quantum system formalism described in the Appendix, the operators acting on the system (i.e., the Pauli matrices) must be expressed in the energy eigenstates basis (with respect to H_0). Therefore, new coordinate system $(\hat{e}_\perp, \hat{e}_y, \hat{e}_\parallel)$ is defined, where $\hat{e}_\parallel = (\sin\phi, 0, \cos\phi)$ is the already introduced unit vector parallel to the quantization axis, $\hat{e}_\perp = (\cos\phi, 0, -\sin\phi)$ is orthogonal to the quantization axis, and $\hat{e}_y = (0, 1, 0)$ has direction along y axis. Now, $\sigma_x^{(\mathrm{h})}$ and $\sigma_z^{(\mathrm{h})}$ can be represented in terms of $\sigma_\perp^{(\mathrm{h})} = \hat{e}_\perp \cdot \boldsymbol{\sigma}^{(\mathrm{h})}$ and $\sigma_0^{(\mathrm{h})} = \hat{e}_\parallel \cdot \boldsymbol{\sigma}^{(\mathrm{h})}$,

$$\sigma_x^{(\mathrm{h})} = \sigma_0^{(\mathrm{h})} \sin\phi + \sigma_\perp^{(\mathrm{h})} \cos\phi, \quad \sigma_y^{(\mathrm{h})}, \quad \sigma_z^{(\mathrm{h})} = \sigma_0^{(\mathrm{h})} \cos\phi - \sigma_\perp^{(\mathrm{h})} \sin\phi.$$

The next step is to define rising and lowering operators with respect to quantization axis $\hat{e}_\parallel$,

$$\begin{aligned} \sigma_+^{(\mathrm{h})} &= \frac{1}{2}(\sigma_\perp^{(\mathrm{h})} + i\sigma_y^{(\mathrm{h})}) = |+\rangle\langle-|, \\ \sigma_-^{(\mathrm{h})} &= \frac{1}{2}(\sigma_\perp^{(\mathrm{h})} - i\sigma_y^{(\mathrm{h})}) = |-\rangle\langle+|. \end{aligned}$$

The spin-environment interaction Hamiltonian may now be written in the useful form

$$H_{\mathrm{int}} = \sigma_+^{(\mathrm{h})} R_-^{(\mathrm{h})} + \sigma_-^{(\mathrm{h})} R_+^{(\mathrm{h})} + \sigma_0^{(\mathrm{h})} R_0^{(\mathrm{h})}, \tag{2.17}$$

where the new environment operators $R_-^{(\mathrm{h})}$, $R_+^{(\mathrm{h})}$ and $R_0^{(\mathrm{h})}$ are definied by

$$\begin{aligned} R_-^{(\mathrm{h})} &= R_x^{(\mathrm{h})} \cos\phi - iR_y^{(\mathrm{h})} - R_z^{(\mathrm{h})} \sin\phi, \\ R_+^{(\mathrm{h})} &= R_x^{(\mathrm{h})} \cos\phi + iR_y^{(\mathrm{h})} - R_z^{(\mathrm{h})} \sin\phi \quad = \quad \left(R_-^{(\mathrm{h})}\right)^\dagger, \\ R_0^{(\mathrm{h})} &= R_x^{(\mathrm{h})} \sin\phi + R_z^{(\mathrm{h})} \cos\phi. \end{aligned} \tag{2.18}$$

One may have the wrong impression, that the interaction Hamiltonian could be written in the form from Eq. (2.17) from the very beginning, with some undefinied environment

operators $R_-^{(\mathrm{h})}$, $R_+^{(\mathrm{h})}$ and $R_0^{(\mathrm{h})}$. However, assuming that the spectral densities of the environment operators have the symmetry of the investigated structure, a big simplification is obtained (as shown later in this section). Therefore it is good to express $R_-^{(\mathrm{h})}$, $R_+^{(\mathrm{h})}$ and $R_0^{(\mathrm{h})}$ as functions of operators $R_x^{(\mathrm{h})}$, $R_y^{(\mathrm{h})}$ and $R_z^{(\mathrm{h})}$, connected with the structure orientation [Eq. (2.18)]. Having properly defined the interaction Hamiltonian, the general form of the dissipator from the Appendix [see Eq. (A.13)] can now be used to obtain the hole dissipator of investigated system,

$$\begin{aligned}\mathcal{L}_{\mathrm{h}}[\rho] &= -\pi \textstyle\sum_{lj} \left[R_{lj}^{(\mathrm{h})}(\omega_j)\left(\sigma_l^{(\mathrm{h})}\sigma_j^{(\mathrm{h})}\rho - \sigma_j^{(\mathrm{h})}\rho\sigma_l^{(\mathrm{h})}\right)\right.\\ &\quad \left. +R_{lj}^{(\mathrm{h})}(-\omega_l)\left(\rho\sigma_l^{(\mathrm{h})}\sigma_j^{(\mathrm{h})} - \sigma_j^{(\mathrm{h})}\rho\sigma_l^{(\mathrm{h})}\right)\right],\end{aligned} \tag{2.19}$$

where $l, j = \pm, 0$, $\omega_0 = 0$, $\omega_+ = -\omega_- = \omega_{\mathrm{h}}$ and the spectral densities for the hole reservoir are defined as [see Eq. (A.9)]

$$R_{lj}^{(\mathrm{h})}(\omega) = \frac{1}{2\pi\hbar^2}\int dt e^{i\omega t}\langle R_l^{(\mathrm{h})}(t) R_j^{(\mathrm{h})}\rangle, \quad l, j = \pm, 0,$$

with the explicit time dependency denoting the operator in the interaction picture with respect to the environment Hamiltonian. Additional simplification of spectral densities can be obtained by employing the system $C_{4\mathrm{v}}$ symmetry and setting $R_{\alpha\beta}^{(\mathrm{h})}(\omega) = 0$ for $\alpha, \beta = x, y, z$, $\alpha \neq \beta$ and $R_{yy}^{(\mathrm{h})}(\omega) = R_{xx}^{(\mathrm{h})}(\omega)$. Then, they are expressed by

$$\begin{aligned}R_{00}^{(\mathrm{h})}(\omega) &= R_{\mathrm{xx}}^{(\mathrm{h})}(\omega)\sin^2\phi + R_{\mathrm{zz}}^{(\mathrm{h})}(\omega)\cos^2\phi,\\ R_{++}^{(\mathrm{h})}(\omega) &= R_{--}^{(\mathrm{h})}(\omega) = \left(R_{\mathrm{zz}}^{(\mathrm{h})}(\omega) - R_{\mathrm{xx}}^{(\mathrm{h})}(\omega)\right)\sin^2\phi,\\ R_{+-}^{(\mathrm{h})}(\omega) &= R_{-+}^{(\mathrm{h})}(\omega) = R_{\mathrm{xx}}^{(\mathrm{h})}(\omega)\left(1+\cos^2\phi\right) + R_{\mathrm{zz}}^{(\mathrm{h})}(\omega)\sin^2\phi,\\ R_{0+}^{(\mathrm{h})}(\omega) &= R_{+0}^{(\mathrm{h})}(\omega) = R_{0-}^{(\mathrm{h})}(\omega) = R_{-0}^{(\mathrm{h})}(\omega) = \left(R_{\mathrm{xx}}^{(\mathrm{h})}(\omega) - R_{\mathrm{zz}}^{(\mathrm{h})}(\omega)\right)\sin\phi\cos\phi.\end{aligned}$$

As mentioned before, trion dissipator $\mathcal{L}_{\mathrm{t}}$ can be obtained from Eq. (2.19) after apprioprate substitutions.

The trion radiative decay is accounted for also by the Lindblad superoperator

$$\begin{aligned}L_{\mathrm{r}}[\rho] &= \gamma_1\left[\sigma_-^{(\uparrow)}\rho\sigma_+^{(\uparrow)} - \frac{1}{2}\left\{\sigma_+^{(\uparrow)}\sigma_-^{(\uparrow)}, \rho\right\}_+ + \sigma_-^{(\downarrow)}\rho\sigma_+^{(\downarrow)} - \frac{1}{2}\left\{\sigma_+^{(\downarrow)}\sigma_+^{(\downarrow)}, \rho\right\}_+\right]\\ &\quad +\frac{1}{2}\gamma_0\left[\sigma_0\rho\sigma_0 - \frac{1}{2}\left\{\sigma_0^2, \rho\right\}_+\right],\end{aligned} \tag{2.20}$$

where γ_1 is the radiative decay rate, γ_0 is the additional pure dephasing rate, and the transition operators are

$$\begin{aligned}\sigma_+^{(\uparrow)} &= \left[\sigma_-^{(\uparrow)}\right]^\dagger = |\uparrow\rangle\langle T\uparrow|,\\ \sigma_+^{(\downarrow)} &= \left[\sigma_-^{(\downarrow)}\right]^\dagger = |\downarrow\rangle\langle T\downarrow|,\\ \sigma_0 &= |T\uparrow\rangle\langle T\uparrow| + |T\downarrow\rangle\langle T\downarrow| - |\uparrow\rangle\langle\uparrow| - |\downarrow\rangle\langle\downarrow|.\end{aligned} \tag{2.21}$$

In order to describe the spin dynamics of the system one has to solve the Eq. (2.15) with the dissipators given by Eqs. (2.19) and (2.20) for the initial density matrix ρ_2, described by Eqs. (2.10) and (2.13). However, it is much easier and more transparent to describe the evolution again in terms of the dynamical variables, corresponding to quantities of interest: $\Sigma_{\rm h}$, $X_{\rm h}$, $Y_{\rm h}$, $N_{\rm t}$, $\Sigma_{\rm t}$, with the initial condition given by components of $\boldsymbol{S}_2$ (remembering that initially trion population is completely polarized, i.e., the initial conditions for $N_{\rm t}$ and $\Sigma_{\rm t}$ are the same and equal to $\Sigma_{\rm t}^{(2)}$). Variables $N_{\rm h}$, $X_{\rm t}$, $Y_{\rm t}$ can be omitted, because the former one is a simple function of $N_{\rm t}$ [Eq. (2.1)] and the latter ones are initially equal to 0 and do not evolve. Evolution equations for the dynamical variables are obtained with the use of the operators defined by Eqs. (2.1)-(2.3) and the density matrix evolution equation,

$$\dot{\hat{A}} = \mathrm{Tr}\left(\hat{A}\dot{\rho}(t)\right), \quad \hat{A} = \hat{\Sigma}_{\rm h}, \hat{X}_{\rm h}, \hat{Y}_{\rm h}, \hat{N}_{\rm t}, \hat{\Sigma}_{\rm t}.$$

Before writing down the evolution equations explicitly the crucial approximation for the trion spin dynamics is made, which simplifies the equation for the trion polarization. Namely, it is assumed that the radiative decay rate γ_1 is much larger than any trion decoherence rates, therefore the trion dissipative dynamics can be described, with a good approximation, as governed only by the recombination processes. With this assumption, the obtained differential equations for trion dynamical variables are easily solved and their solutions are given by

$$\begin{aligned} N_{\rm t}(t) &= N_{\rm t}(0)e^{-\gamma_1 t}, \\ \Sigma_{\rm t}(t) &= \Sigma_{\rm t}(0)e^{-\gamma_1 t}\left[\cos^2\theta + \sin^2\theta\cos\omega_{\rm t}t\right]. \end{aligned} \tag{2.22}$$

For the hole variables, the dynamics is governed by the following set of differential equations

$$\begin{aligned} \dot{\widetilde{\Sigma}}_{\rm h} &= -\left[\frac{3+\cos 2\phi}{2}\kappa_x + \frac{1-\cos 2\phi}{2}\kappa_{x0}\right]\widetilde{\Sigma}_{\rm h} - \left(\frac{\kappa_x-\kappa_{x0}}{2}\right)\sin 2\phi\widetilde{X}_{\rm h} \\ &\quad -\omega_{\rm h}\sin\phi Y_{\rm h} - 2\kappa_x'\cos\phi N_{\rm t} + \gamma_1\Sigma_{\rm t}, \end{aligned} \tag{2.23}$$

$$\begin{aligned} \dot{\widetilde{X}}_{\rm h} &= -\frac{\kappa_z-\kappa_{z0}}{2}\sin 2\phi\widetilde{\Sigma}_{\rm h} - \left[\frac{1-\cos 2\phi}{2}\kappa_z + \frac{1+\cos 2\phi}{2}\kappa_{z0} + \kappa_x\right]\widetilde{X}_{\rm h} \\ &\quad +\omega_{\rm h}\cos\phi Y_{\rm h} + (\kappa_x'-\kappa_z')\sin\phi N_{\rm t}, \end{aligned} \tag{2.24}$$

$$\begin{aligned} \dot{Y}_{\rm h} &= \omega_{\rm h}\sin\phi\widetilde{\Sigma}_{\rm h} - \omega_{\rm h}\cos\phi\widetilde{X}_{\rm h} \\ &\quad -\left[\frac{1+\cos 2\phi}{2}(\kappa_{z0}+\kappa_x) + \frac{1-\cos 2\phi}{2}(\kappa_{x0}+\kappa_z)\right]Y_{\rm h}, \end{aligned} \tag{2.25}$$

where new hole variables $\widetilde{\Sigma}_{\rm h} = \Sigma_{\rm h} - \Sigma_{\rm h}^{(\rm eq)}$ and $\widetilde{X}_{\rm h} = X_{\rm h} - X_{\rm h}^{(\rm eq)}$ with subtracted equilibrium

values [given by Eq. (2.8)] are used and the decoherence rates are defined as

$$\begin{aligned}
\kappa_x &= 2\pi\left[R_{xx}(\omega_\mathrm{h}) + R_{xx}(-\omega_\mathrm{h})\right], & \kappa_z &= 2\pi\left[R_{zz}(\omega_\mathrm{h}) + R_{zz}(-\omega_\mathrm{h})\right], \\
\kappa'_x &= 2\pi\left[R_{xx}(\omega_\mathrm{h}) - R_{xx}(-\omega_\mathrm{h})\right], & \kappa'_z &= 2\pi\left[R_{zz}(\omega_\mathrm{h}) - R_{zz}(-\omega_\mathrm{h})\right], \\
\kappa_{x0} &= 4\pi R_{xx}(0), & \kappa_{z0} &= 4\pi R_{zz}(0).
\end{aligned} \tag{2.26}$$

Note that due to the lock-in technique used in the experiment, only the Kerr rotation change induced by the pump beam is measured, therefore what is experimentally accesible is $\widetilde{\Sigma}_\mathrm{h}$, not Σ_h. The set of differential equations 2.23-2.25 can be solved by inserting the solutions for the trion variables [Eq. (2.22)] and using the Laplace transform method. In general, the Lindblad evolution can be again written as the transformation of the vector $\boldsymbol{S}_2$ into vector $\boldsymbol{S}_3(t)$, corresponding to density matrix $\rho(t)$,

$$\boldsymbol{S}_3(t) = \begin{pmatrix} \Sigma_\mathrm{h}(t) \\ X_\mathrm{h}(t) \\ Y_\mathrm{h}(t) \\ \Sigma_\mathrm{t}(t) \end{pmatrix} = \hat{A}_\mathrm{L}(t)\boldsymbol{S}_2 + \boldsymbol{b}_\mathrm{L}(t). \tag{2.27}$$

2.5 Repetitive evolution in the RSA experiment

In the RSA experiment, the system undergoes the three-step evolution described in secs. 2.2-2.4 repetetively, with the time period t_rep given by the repetition rate of the pumping laser (see Fig. 2.2). In this case, the spin polarization surviving between subsequent laser repetitions is essential. Therefore, in order to find the resonantly amplified spin polarization just before the arrival of the pump pulse (which corresponds to the RSA signal), the fixed point of the three-step transformation (pump pulse, fast decoherence, and Lindblad evolution during the repetition interval t_rep) is found:

$$A_\mathrm{L}(t_\mathrm{rep})\left(A_\mathrm{fd}\left(A_\mathrm{p}\boldsymbol{S} + B_\mathrm{p} - \boldsymbol{S}^{(\mathrm{eq})}\right) + \boldsymbol{S}^{(\mathrm{eq})}\right) + \boldsymbol{b}_\mathrm{L}(t_\mathrm{rep}) = \boldsymbol{S}. \tag{2.28}$$

As the measurement accounts only for the Kerr rotation change induced by the pump beam, in order to model the experimentally obtained signal the equilibrium values of the dynamical variables must be subtracted at the end, i.e., to describe the RSA signal $\boldsymbol{S} - \boldsymbol{S}^{(\mathrm{eq})}$ vector is used, not just $\boldsymbol{S}$. To simplify the obtained formula for the stationary vector $\boldsymbol{S} - \boldsymbol{S}^{(\mathrm{eq})}$ it is assumed that the hole spin dephasing rates are small compared to the trion recombination rate, which is justified by the condition of long SDT in the RSA measurements. Additionaly, in order to simulate the response from an inhomogeneous ensemble of hole spins, the obtained result is averaged according to a Gaussian distribution of hole g-factors with the standard deviation Δg.

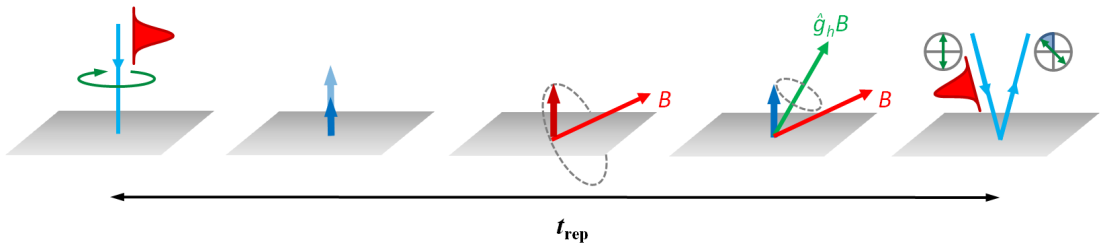

Figure 2.2: Repetitive evolution the system undergoes with the period t_{rep} in the RSA experiment: pumping, fast hole decoherence, and actual evolution (precession, decoherence, and recombination).

2.6 Interaction with the probe pulse

After the arrival of the pump pulse, the system evolves for the time τ according to the description given in sec. 2.4. Then, the linearly polarized probe pulse arrives at the sample surface. After reflection, due to the magnetooptical Kerr effect, its polarization plane is rotated, and the rotation angle yields the information about the spin polarization present in the sample at the arrival of the probe pulse. In this section, the microscopic origin of this effect will be presented, i.e. the relation between the measured TRKR signal and the elements of the density matrix, at the moment when the probe pulse arrives, will be established [16].

To focus attention, the probe pulse is chosen to be linearly polarized along the x axis,

$$\boldsymbol{\mathcal{E}}(t) = \frac{\boldsymbol{\mathcal{E}}_0}{2}\eta\left(\frac{t-\tau}{\tau_{\mathrm{p}}}\right)e^{-i\omega_{\mathrm{p}}(t-\tau)+i\psi} + \text{c.c.}, \quad \boldsymbol{\mathcal{E}}_0 = \mathcal{E}_0\begin{pmatrix}1\\0\\0\end{pmatrix},$$

where $\eta[(t-\tau)/(\tau_{\mathrm{p}})] = \exp[-[(t-\tau)/\tau_{\mathrm{p}}]^2/2]$ is the Gaussian pulse shape of length τ_{p}, delayed by τ in relation to the pump pulse. The electric field is assumed to couple to the interband transitions via a dipole moment $\boldsymbol{d}$, similarly as the pump pulse, but now the influence of the detuning is neglected. Then, the relevant Hamiltonian (in the reference frame rotating with transition frequency ω and using the rotating wave and dipole approximations) is given by

$$H_{\mathrm{probe}} = \frac{1}{2\sqrt{2}}f(t-\tau)e^{-i\psi}\left(|\uparrow\rangle\langle T\uparrow| + |\downarrow\rangle\langle T\downarrow|\right) + \text{H.c.}, \tag{2.29}$$

where $f(t-\tau) = -\boldsymbol{d}\cdot\boldsymbol{\mathcal{E}}_0^*(1+r)\eta[(t-\tau)/\tau_{\mathrm{p}}]$ is the envelope function.

The total field, coming from the probe pulse after reflection from the sample, can be projected onto the two axes x, y, oriented at 45° with respect to the original polarization

of the probe beam. Then, the measured rotation of the polarization axis is given by the difference of intensity between the corresponding two components of the field,

$$\Delta I = \frac{1}{\mu_0 c}\left[\langle E_y^2(t)\rangle - \langle E_x^2(t)\rangle\right] = \frac{1}{\mu_0 c}\,\mathrm{Im}\left(E_+ E_-^*\right), \tag{2.30}$$

where E_+ and E_- are the amplitudes of the circularly polarized components (right- and left- polarized, respectively) of the total field and time averaging over the period of the electromagnetic field is denoted by $\langle\cdot\rangle$. The total field originates from two sources: the reflection at the surface of the capping layer, E_R (which will be treated on the macroscopic level), and the field emitted by the nanostructure, E_S. Taking this into account, the circularly polarized components of the total field can be written as:

$$E_\pm = E_{\mathrm{R}\pm} + E_{\mathrm{S}\pm}. \tag{2.31}$$

Since the reflected component of the linearly polarized field simply follows the pulse envelope the amplitudes of its σ_+ and σ_- components at the sample surface are equal:

$$E_{\mathrm{R}\pm}(t) = E_\mathrm{R}(t) = \frac{1}{\sqrt{2}} r\mathcal{E}_0\eta\left(\frac{t-\tau}{\tau_\mathrm{p}}\right)e^{-i\psi}. \tag{2.32}$$

The field emitted by the nanostructure, E_S, originates from the interband polarization. The dipole moment, coming from every hole-trion superposition, can be decomposed into the circularly right- and left-polarized components,

$$\pi_+ = d\langle T\uparrow|\rho(t)|\uparrow\rangle e^{-i\omega t} + \text{c.c.}, \tag{2.33}$$

$$\pi_- = d\langle T\downarrow|\rho(t)|\downarrow\rangle e^{-i\omega t} + \text{c.c.}, \tag{2.34}$$

which results in the polarization currents

$$\mathcal{J}_+ = \nu\frac{\partial\pi_+}{\partial t} = -i\nu\omega d\langle T\uparrow|\rho(t)|\uparrow\rangle e^{-i\omega t} + \text{c.c.}, \tag{2.35}$$

$$\mathcal{J}_- = \nu\frac{\partial\pi_-}{\partial t} = -i\nu\omega d\langle T\downarrow|\rho(t)|\downarrow\rangle e^{-i\omega t} + \text{c.c.}, \tag{2.36}$$

where ν is the area density of trapped holes. Therefore, the the radiation emitted from the structure, at the sample surface, is given by

$$\begin{pmatrix} E_{\mathrm{S}+}(t) \\ E_{\mathrm{S}-}(t) \end{pmatrix} = \frac{i}{2}\mu_0 c\nu d\omega \begin{pmatrix} \langle T\uparrow|\rho(t)|\uparrow\rangle \\ \langle T\downarrow|\rho(t)|\downarrow\rangle \end{pmatrix} e^{-i\varphi}, \tag{2.37}$$

where the phase shift (with respect to the field reflected at the surface, E_R), $\varphi = 2D\omega n/c$, comes from the propagation through the capping layer of width D.

Now, one can obtain the expression for the measured signal by substituting Eqs. (2.32) and (2.37) into Eq. (2.31) and then into Eq. (2.30). After retaining only terms of the first order in the nanostructure response, $E_{\mathrm{S}\pm}$, the TRKR signal is given by

$$\Delta I(t) = \frac{1}{2}\nu\omega d\,\mathrm{Re}\left[E_\mathrm{R}^*(t)\langle T\uparrow|\rho(t)|\uparrow\rangle e^{-i\varphi} - E_\mathrm{R}(t)\langle T\downarrow|\rho(t)|\downarrow\rangle^* e^{i\varphi}\right]. \tag{2.38}$$

The above equation describes the experimentally measured signal in terms of the quantum state of the system. Therefore, the next step is to find out how the probe pulse affects the system state, i.e., how the measured signal is connected with the state just before the arrival of the probe pulse $\rho(\tau^-)$ (τ^- denotes the time instant just before the arrival of the probe pulse).

In order to do this in an analytical way, the following assumptions are made. First, the probe pulse duration is assumed to be shorter than any relevant time scale of the system dynamics. Secondly, the dephasing times of interband coherences are assumed to be longer than the pulse duration. Then, one can completely neglect the system evolution during the pulse. Using the introduced Hamiltonian [Eq. (2.29)] and taking into account that the state of the system $\rho(t)$ is prepared by the probe pulse from the state $\rho(\tau^-)$, the system density matrix is transformed according to:

$$\rho(t) = W(t)\rho(\tau^-)W^\dagger(t),$$

where $W(t)$ is an unitary evolution operator given by

$$W(t) = \cos\frac{\Phi(t)}{2}\mathbb{I} - i\sin\frac{\Phi(t)}{2}\left[\left(|\uparrow\rangle\langle T\uparrow| + |\downarrow\rangle\langle T\downarrow|\right)e^{i\psi} + \text{H.c.}\right], \tag{2.39}$$

and

$$\Phi(t) = \frac{1}{\sqrt{2}\hbar}\int_{-\infty}^{t} ds f\left(\frac{s-\tau}{\tau_\text{p}}\right). \tag{2.40}$$

Having the evolution operator, it is straightforward to find the interband matrix elements (for $\sigma = \uparrow, \downarrow$):

$$\begin{aligned}\langle T\sigma|\rho(t)|\sigma\rangle &= \cos^2\frac{\Phi(t)}{2}\langle T\sigma|\rho(\tau^-)|\sigma\rangle + \sin^2\frac{\Phi(t)}{2}\langle\sigma|\rho(\tau^-)|T\sigma\rangle e^{-2i\psi} \\ &\quad + \frac{i}{2}\sin\Phi(t)\left[\langle T\sigma|\rho(\tau^-)|T\sigma\rangle - \langle\sigma|\rho(\tau^-)|\sigma\rangle\right]e^{-i\psi}.\end{aligned} \tag{2.41}$$

Finally, assuming that the interband dephasing time is much shorter than the delay time τ between the pump and probe pulse, one can neglect the interband matrix elements at time τ^- in Eq. (2.41). Then, substituting it into Eq. (2.38), with the use of Eq. (2.32), one obtains the expression for the Kerr signal:

$$\Delta I = \frac{1}{4\sqrt{2}} r\mathcal{E}\eta\left(\frac{t-\tau}{\tau_\text{p}}\right)\nu\omega d\sin\varphi\sin\Phi(t)\left[\Sigma_\text{t}(\tau^-) - \Sigma_\text{h}(\tau^-)\right]. \tag{2.42}$$

Ignoring the factors that cannot be directly measured experimentally and integrating over time, in order to obtain integrated detection signal, one arrives at the TRKR signal

$$\text{TRKR} \sim \Sigma_\text{t}(\tau^-) - \Sigma_\text{h}(\tau^-). \tag{2.43}$$

This way, the TRKR measurement gives access to the evolution of the spin polarizations in the system.

Chapter 3

Microscopic modelling of decoherence

This chapter is devoted to the studies of microscopic origin of the hole spin decoherence in the investigated system, i.e. the p-doped quantum well. The usual explanation for the decrease of spin lifetimes with increasing temperature is that the localized holes become free carriers due to the thermal release from the localization centres and, because of the spin-orbit coupling, very efficient spin decoherence mechanisms start working, e.g., resulting from the D'yakonov-Perel' mechanism [18]. Therefore, spin polarization observed experimentally (Kerr signal) originates only from the localized states and should vanish when all the carriers become thermally released. In this chapter, it is shown that it may not be the decrease of occupation of localized states, but the spin exchanging interaction between the localized and released (free) states that is mainly responsible for the decrease of the spin life-times. First, the model of localized holes is extended to account for the final depth of localization potentials by introducing the thermally released states. Next, the model of the interaction between localized and free states is presented. Finally, the Coulomb interaction between the thermally relased and localized states is studied and the interaction induced spin-flip probability of the localized hole state is calculated in the Fermi's Golden Rule approach.

3.1 Extended model with thermally released holes

The considered system consists of holes confinied in a quasi-two-dimensional structure, i.e., it is assumed that the energies (temperatures) involved are small enough to restrict the description to the lowest out-of-plane QW energy level. As mentioned in the former chapter, due to the QW width fluctuations a number of localization centres exist in the structure. Therefore, there are two kinds of available states for the holes: localized and

free ones. The considered particles (holes) are fermions, therefore they obey Fermi-Dirac statistics,

$$N = \sum_i \frac{1}{\exp(\beta(E_i - \mu)) + 1}, \tag{3.1}$$

where N is the number of particles in the system, μ is the chemical potential, $\beta = 1/k_{\mathrm{B}}T$ is the inverse temperature and the index i goes over all the energy levels E_i in the system. To make the explicit distinction between two kinds of available states, Eq. (3.1) may be rewritten in the form

$$N = \sum_\alpha \frac{1}{\exp(\beta(E_\alpha - \mu)) + 1} + \sum_{\boldsymbol{p}} \frac{1}{\exp(\beta(\frac{p^2}{2m} - \mu)) + 1}, \tag{3.2}$$

where the summation over α corresponds to the set of localized states and the energy of the released (free) states has been written explicitly, i.e., dependent on the momentum $\boldsymbol{p}$. Due to the random character of the localization centres (fluctuations of the QW width), their energies are assumed to be normally distributed around $E_0 < 0$ with the standard deviation σ_E. The next step is to change the summation into 2-dimensional integration,

$$\sum_{\boldsymbol{p}} \to \frac{2S}{(2\pi\hbar)^2} \int d^2p \to \frac{Sm}{\pi\hbar^2} \int dE,$$

$$\sum_\alpha \to \frac{N_{\mathrm{QD}}}{\sqrt{2\pi}\sigma_E} \int \exp\left(-\frac{(E - E_0)^2}{2\sigma_E^2}\right) dE,$$

where S is the surface of the QW, N_{QD} is the number of localization centers, m is the hole mass and the factor 2 appears before the first integral because of the spin summation. One then arrives at the expression for the concentration,

$$n = \frac{n_{\mathrm{QD}}}{\sqrt{2\pi}\sigma_E} \int_{-\infty}^{\infty} dE \frac{\exp(-\frac{(E-E_0)^2}{2\sigma_E^2})}{\exp(\beta(E - \mu) + 1} + \frac{m}{\beta\pi\hbar^2} \ln(1 + e^{\beta\mu}), \tag{3.3}$$

where n_{QD} is the concentration of the localization centers. Eq. (3.3) can be solved numerically to obtain the chemical potential μ for different concentrations n, n_{QD} and localization centres distribution parameters E_0, σ_E. Using the calculated chemical potential one can then find the distribution function for the free holes

$$f(E) = \left(e^{\beta(E-\mu)} + 1\right)^{-1}, \tag{3.4}$$

which will be used in the next section for the calculations of the total spin-exchanging scattering probabilities between free and localized states.

It is also useful to introduce the parameter $x = n_{\mathrm{QD}}/n$, which describes how many localization centres there are on average per one hole. The schematic graphs in Fig. 3.1 show 4 possible situations for the value of chemical potential, depending on the concentration of holes for $T = 0$. Due to the fact that experimentally all the holes are observed

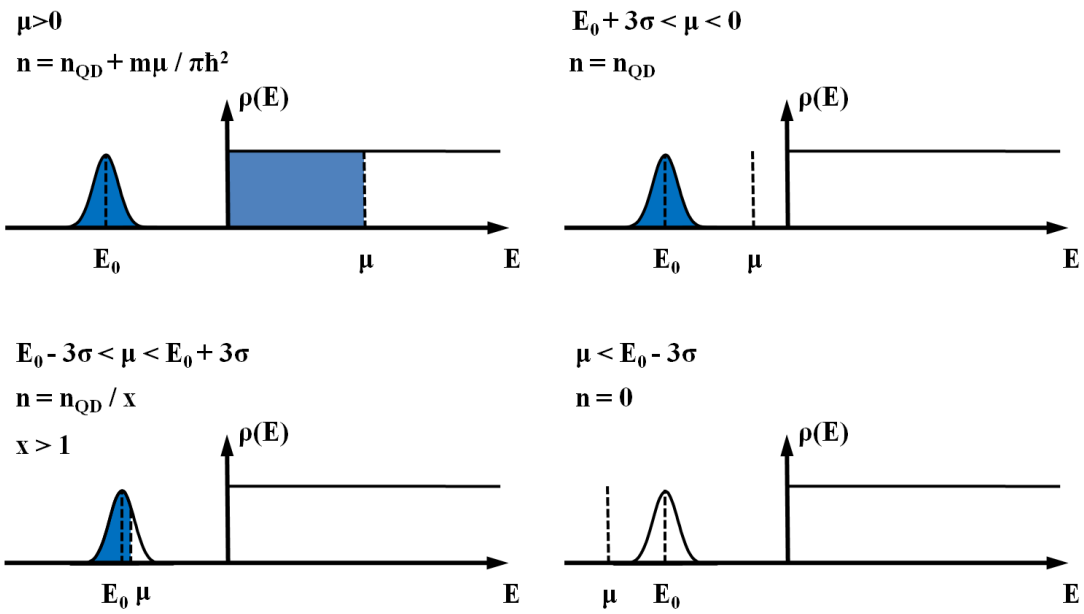

Figure 3.1: The plots schematically show densities of states (black lines) and the occupied states (blue fill) in four regions of the chemical potential values and the corresponding values of concentration at zero temperature.

to be localized in low temperatures, $x \geq 1$ (there is at least the same number of localization centres as carriers) and it is the bottom left graph in Fig. 3.1 that represents real situation.

3.2 Interaction between free and localized hole states

3.2.1 Model

Having the distribution function for the free holes given by Eq. (3.4) [with the chemical potential obtained from numerical solution of Eq. (3.3)], one can now calculate the interaction between the free states and the localized ones. It is assumed that the concentration of localization centres is small enough, i.e., the average distance between them is big enough, to neglect the interaction between localized states. Therefore, only a single impurity (situated at the origin of the coordinate system) is considered, with a single hole localized on it (more than one hole is not favourable due to the Coulomb repulsion). For the hole on the impurity, normalized Gaussian shape (with anisotropic out-of-plane component) of the ground state wavefunction $\Phi(\boldsymbol{r})$ is assumed,

$$\Phi(\boldsymbol{r}) = \frac{1}{\sqrt{\pi}\sigma} e^{-\frac{\rho^2}{2\sigma^2}} \cdot \frac{1}{(\sqrt{\pi}\sigma_z)^{\frac{1}{2}}} e^{-\frac{z^2}{2\sigma_z^2}}, \tag{3.5}$$

where σ and σ_z are the parameters describing the in-plane and out-of-plane Gaussian width, respectively (which will be estimated later), and the cylindrical coordinates $\rho = \sqrt{x^2+y^2}$ and z are used (the system has cylindrical symmetry). Two-dimensional free hole gas is described by the product of the free hole wavefunctions (2D plane waves with the normalization factor taken from the assumption of finite surface S and wave vector: $\boldsymbol{k}_{\parallel} = \boldsymbol{k} = [k_x, k_y, 0]$) with the Gaussian envelope along $\hat{z}$ (out of the QW plane),

$$\Psi_{\boldsymbol{k}}(\boldsymbol{r}) = \frac{1}{\sqrt{S}} e^{i\boldsymbol{k}\cdot\boldsymbol{\rho}} \cdot \frac{1}{(\sqrt{\pi}\sigma_z)^{\frac{1}{2}}} e^{-\frac{z^2}{2\sigma_z^2}}. \tag{3.6}$$

Each state ($\Phi(\boldsymbol{r})$, $\Psi_{\boldsymbol{k}}(\boldsymbol{r})$) has also a spin component: $\uparrow$ or $\downarrow$.

As the localization centres originate from completely random structural factors (QW width fluctuations) it is hard to determine the widths of the Gaussian wavefunction σ and σ_z (they depend on the depth and size of the unkown localization potential). However, one can estimate the approximate value of σ and σ_z in the following way. First, the assumption is made that the confining potential of the QW is an infinite (square) quantum well along z direction. This approach is justified, because for a thin QW (4nm wide, in the experiments performed by the Regensburg group) the confinment should play a dominant role. What is more, the same z dependence of the wavefunctions of localized and free holes (the same σ_z) was already assumed, which suggests that localization centres only slightly influence the potential along the z direction. Now, the real ground state in an infinite quantum well has the cosine shape, however it can approximated with a Gaussian. This is done, by comparison of the energy of the ground state in the infinite well of width a:

$$E_{z\infty} = \frac{\hbar^2\pi^2}{8ma^2},$$

with the energy of a free Gaussian wavefunction (the kinetic part):

$$E_z = \frac{\hbar^2}{4m\sigma_z^2},$$

which gives:

$$\sigma_z = \frac{\sqrt{2}}{\pi} a. \tag{3.7}$$

Next, it is known that at small temperatures all holes are trapped, so $n_{\mathrm{QD}} \geq n$. As the localized hole-localized hole interaction was neglected, the mean distance between localization centres, $l = (n_{\mathrm{QD}})^{-\frac{1}{2}}$, should fulfill the inequality is $l > 4\sigma$ (the factor 4 was used, because for the separation of two Gaussian wavefunctions by 4σ the overlap is smaller than 2.25%). Therefore, $\sigma < 1/(4\sqrt{n})$. On the other hand, it is expected that $\sigma > \sigma_z$, because σ_z is mainly determined by the confinment. Alltogether, the following approximate constraints are obtained for σ,

$$\frac{\sqrt{2}}{\pi} a < \sigma < \frac{1}{4\sqrt{n}}. \tag{3.8}$$

The interaction between free and localized states has a twofold nature. First, the free carrier can scatter on the impurity and exchange the spin. Then, the spin information transfered from the localized to the free carrier is quickly lost (due to the very short spin lifetimes of free carriers), which effectively results in decrease of the spin polarization in the sample. On the other hand, the Coulomb potential of the localized state influences the density of states of free carriers. This results in two phenomena that can decrease the scattering probability. First, due to the repulsive potential the probability of finding a free carrier should decrease in the neighbourhood of the localized hole. Secondly, the localized becomes effectively screened. Here, the approximation that includes only the first effect of the interaction, i.e. spin-exchanging scattering, will be discussed.

3.2.2 Spin-flip probabilities

The transition probability from the initial state $|i\rangle$, with a localized spin-up hole and a free spin-down hole with wave vector $\boldsymbol{k}'$, to any of the allowed states with a localized spin-down hole $|f\rangle$ (due to the conservation of spin the final free hole state must be spin-up) will be calculated. All the calculations will be performed in the absence of magnetic field (no favoured spin axes) so the transition probabilities up-down ($\uparrow$ to $\downarrow$) and down-up ($\downarrow$ to $\uparrow$) for the localized state should be the same (the up-down transition was chosen only to focus the attention). The initial $|i\rangle$ and final $|f\rangle$ states can be described in the second quantization formalism

$$\begin{aligned} |i\rangle &= a^\dagger_{\boldsymbol{k}'\downarrow} a^\dagger_{\Phi\uparrow}|0\rangle, \\ |f\rangle &= a^\dagger_{\boldsymbol{k}\uparrow} a^\dagger_{\Phi\downarrow}|0\rangle, \end{aligned} \tag{3.9}$$

where a_Φ, $a_{\boldsymbol{k}}$ are the annihilation operators for the localized and free states (described by wavefunctions $\Phi(\boldsymbol{r})$ and $\Psi_{\boldsymbol{k}}(\boldsymbol{r})$, respectively), the projection of the spin on the structure axis (perpendicular to the QW plane) is described by $\uparrow$, $\downarrow$ and $|0\rangle$ denotes the vacuum state. Using Fermi's Golden Rule, the transition probability from the initial state $|i\rangle$ to any of the allowed states $|f\rangle$ (conservation of spin and energy is taken into account) can be written as

$$P_{(\boldsymbol{k}'\downarrow,\Phi\uparrow)\to(\boldsymbol{k}\uparrow,\Phi\downarrow)} = \frac{2\pi}{\hbar}\sum_{\boldsymbol{k}} |\langle 0|a_{\Phi\downarrow}a_{\boldsymbol{k}\uparrow}|V|a^\dagger_{\boldsymbol{k}'\downarrow}a^\dagger_{\Phi\uparrow}|0\rangle|^2\delta(E_{\boldsymbol{k}} - E_{\boldsymbol{k}'}), \tag{3.10}$$

where V is the Coulomb interaction operator $V = \frac{1}{2}\sum_{ijkl} V_{ijkl}a^\dagger_i a^\dagger_j a_l a_k$ and the indices i, j, k, l go over all possible states. The only non-vanishing parts of Eq. (3.10) corresponding to the situation when the spin of the trapped hole is flipped, see Fig. 3.2, are the exchange terms

$$\begin{aligned} V_1 &= V_{\Phi k\Phi k'} a^\dagger_{\Phi\downarrow} a^\dagger_{\boldsymbol{k}\uparrow} a_{\Phi\uparrow} a_{\boldsymbol{k}'\downarrow}, \\ V_2 &= V_{k\Phi k'\Phi} a^\dagger_{\boldsymbol{k}\uparrow} a^\dagger_{\Phi\downarrow} a_{\boldsymbol{k}'\downarrow} a_{\Phi\uparrow}. \end{aligned}$$

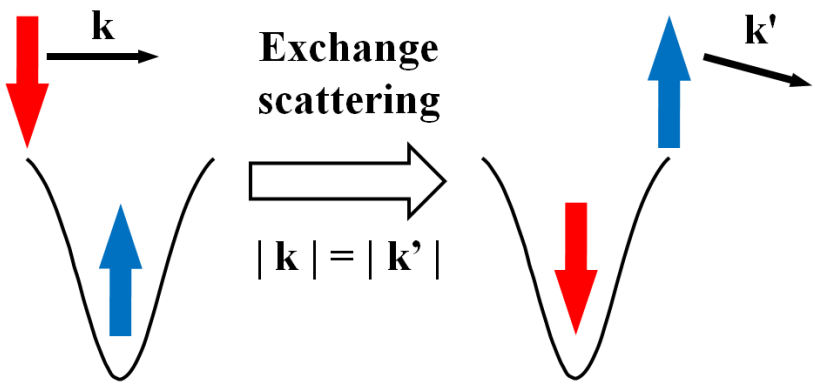

Figure 3.2: Schematic representation of the interaction-induced spin-flip of the localized hole.

The matrix elements are equal, $V_{\Phi k \Phi k'} = V_{k \Phi k' \Phi}$, therefore Eq. (3.10) simplifies and the transition probability is given by

$$P_{(\boldsymbol{k}'\downarrow,\Phi\uparrow)\to(\boldsymbol{k}\uparrow,\Phi\downarrow)} = \frac{2\pi}{\hbar}\sum_{\boldsymbol{k}} |V_{\Phi k \Phi k'}|^2 \delta(E_{\boldsymbol{k}} - E_{\boldsymbol{k}'}). \tag{3.11}$$

The next step is to evaluate the matrix element for the Coulomb interaction:

$$V_{\Phi k \Phi k'} = \frac{e^2}{4\pi\epsilon\epsilon_0}\int d^3r \int d^3r' \Phi^*(\boldsymbol{r})\Psi^*_{\boldsymbol{k}}(\boldsymbol{r}')\frac{1}{|\boldsymbol{r}-\boldsymbol{r}'|}\Phi(\boldsymbol{r}')\Psi_{\boldsymbol{k}'}(\boldsymbol{r}), \tag{3.12}$$

where e is the elementary charge, ϵ_0 is the vacuum permittivity, ϵ is the relative permittivity of the medium (here GaAs). In order to calculate $V_{\Phi k \Phi k'}$ several transformations are applied. First, the Fourier transform of Coulomb potential is used to represent the interaction:

$$\frac{1}{|\boldsymbol{r}-\boldsymbol{r}'|} = \frac{4\pi}{(2\pi)^3}\int d^3q \frac{e^{i\boldsymbol{q}\cdot(\boldsymbol{r}-\boldsymbol{r}')}}{q^2}. \tag{3.13}$$

Also the fact that the Fourier transform of a Gaussian is another Gaussian is employed:

$$\mathcal{F}\{\Phi(x)\} = \int dx \frac{1}{\sqrt{2\pi}\sigma} e^{-\frac{x^2}{2\sigma^2}} e^{-iqx} = e^{-\frac{q^2\sigma^2}{2}}.$$

Now, denoting $A = e^2/(8\epsilon\epsilon_0 S\pi^5\sigma^2\sigma_z^2)$, inserting the explicit form of the wavefunctions [given by Eqs. (3.5) and (3.6)] and making a distinction between in-plane and out-of-plane component of $\boldsymbol{q}$, $\boldsymbol{q}_{\parallel} = \boldsymbol{q} = [q_x, q_y, 0]$ and q_z, the first step of the calculation can be

performed,

$$\begin{aligned}
V_{\Phi k \Phi k'} &= A \int \frac{d^3q}{q^2+q_z^2} \int d^2\rho e^{-\frac{\rho^2}{2\sigma^2}} e^{-i(-\boldsymbol{k}'-\boldsymbol{q})\cdot\boldsymbol{\rho}} \int d^2\rho' e^{-\frac{\rho'^2}{2\sigma^2}} e^{-i(\boldsymbol{k}+\boldsymbol{q})\cdot\boldsymbol{\rho}'} \\
&\times \int dz e^{-\frac{z^2}{\sigma_z^2}} e^{-i(-q_z z)} \int dz' e^{-\frac{z'^2}{\sigma_z^2}} e^{-iq_z z'} \\
&= 4\pi^3\sigma^4\sigma_z^2 A e^{-\frac{\sigma^2}{2}(k^2+k'^2)} \int \frac{d^3q}{q^2+q_z^2} e^{-\sigma^2 q^2} e^{-\frac{\sigma_z^2}{2}q_z^2} e^{-\sigma^2 \boldsymbol{q}\cdot(\boldsymbol{k}+\boldsymbol{k}')} \\
&= B \int \frac{d^3q}{q^2+q_z^2} e^{-\sigma^2\boldsymbol{q}^2} e^{-\frac{\sigma_z^2}{2}q_z^2} e^{-\sigma^2\boldsymbol{q}\cdot(\boldsymbol{k}+\boldsymbol{k}')},
\end{aligned}$$

where $B = 4\pi^3\sigma^4\sigma_z^2 A \exp(-\sigma^2(k^2+k'^2)/2)$. The next step is to introduce the vector $\boldsymbol{K} = \boldsymbol{k} + \boldsymbol{k'}$ and use cylindrical coordinates with the x axis along $\boldsymbol{K}$ (so that the angle between between $\boldsymbol{q}$ and $\boldsymbol{K}$ is the azimuthal angle ϕ),

$$V_{\Phi k \Phi k'} = B \int_0^{2\pi} d\phi \int_0^\infty dq \cdot q e^{-\sigma^2 q^2} e^{-\sigma^2 qK\cos\phi} \int_0^\infty \frac{dq_z}{q^2+q_z^2} e^{-\frac{\sigma_z^2}{2}q_z^2}.$$

The last integral (along q_z) can be replaced by

$$\int_0^\infty \frac{dq_z}{q^2+q_z^2} e^{-\frac{\sigma_z^2}{2}q_z^2} = \frac{1}{\sqrt{\pi}} \frac{e^{\frac{\sigma_z^2}{2}q^2}}{q} \int_{\frac{\sigma_z}{\sqrt{2}}q}^\infty dt e^{-t^2} = \frac{1}{2}\frac{e^{\frac{\sigma_z^2}{2}q^2}}{q} - \frac{1}{\sqrt{\pi}} \frac{e^{\frac{\sigma_z^2}{2}q^2}}{q} \int_0^{\frac{\sigma_z}{\sqrt{2}}q} dt e^{-t^2},$$

and the expression for the matrix element takes the form of

$$V_{\Phi k \Phi k'} = \frac{B}{2} J_1 - \frac{B}{\sqrt{\pi}} J_2,$$

where the integrals J_1 and J_2 are given by

$$\begin{aligned}
J_1 &= \int_0^{2\pi} d\phi \int_0^\infty dq e^{-\sigma^2 q^2} e^{\frac{\sigma_z^2}{2}q^2} e^{-\sigma^2 qK\cos\phi}, \\
J_2 &= \int_0^{2\pi} d\phi \int_0^\infty dq e^{-\sigma^2 q^2} e^{\frac{\sigma_z^2}{2}q^2} e^{-\sigma^2 qK\cos\phi} \int_0^{\frac{\sigma_z}{\sqrt{2}}q} dt e^{-t^2}.
\end{aligned}$$

First, the integral J_1 will be calculated. Using the definition of the modified Bessel function of the first kind $I_0(x) = \frac{1}{\pi}\int_0^\pi d\phi e^{x\cos\phi}$, the angular part of J_1 can be transformed to

$$\int_0^{2\pi} d\phi e^{-\sigma^2 qK\cos\phi} = 2\pi I_0(\sigma^2 Kq).$$

Now, changing the integration variable to $p = \sigma^2 Kq$, one arrives at the formula for J_1 given by:

$$J_1 = 2\pi \int_0^\infty \frac{dp}{\sigma^2 K} e^{-\frac{\sigma^2 - \frac{\sigma_z^2}{2}}{\sigma^4 K^2}p^2} I_0(p),$$

which can be straightforwardly calculated with the use of the property of the I_0 function,

$$\int_0^\infty dx e^{-ax^2} I_0(x) = \frac{\sqrt{\pi}}{2\sqrt{a}} e^{\frac{1}{8a}} I_0\left(\frac{1}{8a}\right),$$

and give the the analytical expression for the integral J_1,

$$J_1 = \frac{\pi^{\frac{3}{2}}}{\sqrt{\sigma^2 - \frac{\sigma_z^2}{2}}} \exp\left(\frac{\sigma^4 K^2}{8(\sigma^2 - \frac{\sigma_z^2}{2})}\right) I_0\left(\frac{\sigma^4 K^2}{8(\sigma^2 - \frac{\sigma_z^2}{2})}\right). \tag{3.14}$$

Now, the integral J_2 will be calculated. The angular part can be transformed the same way as for J_1 and, by introducing new integration variables $t = \sigma_z q w/\sqrt{2}$ and $p = \sigma^2 K q$, the expression for J_2 takes the form

$$J_2 = \frac{2\pi\sigma_z}{\sqrt{2}\sigma^4 K^2} \int_0^1 dw \int_0^\infty dpp \exp\left(-\frac{\sigma^2 - \frac{\sigma_z^2}{2} + \frac{\sigma_z^2}{2}w^2}{\sigma^4 K^2} p^2\right) I_0(p).$$

Focusing on the integral over p and denoting $C = (\sigma^2 - \frac{\sigma_z^2}{2} + \frac{\sigma_z^2}{2}w^2)/(\sigma^4 K^2)$ one can integrate by parts and obtain

$$\int_0^\infty dppe^{-Cp^2} I_0(p) = \frac{1}{2C}\left(1 + \int_0^\infty dpe^{-Cp^2} I_1(p)\right).$$

Using another equality for the Bessel function,

$$\int_0^\infty dpI_1(p)e^{-Cp^2} = e^{\frac{1}{4C}} - 1$$

the integral over p can be calculated. Finally, inserting it into the expression for J_2 and writing C explicitly, one obtains

$$J_2 = \frac{\pi\sigma_z}{\sqrt{2}} \int_0^1 dw \frac{1}{\sigma^2 - \frac{\sigma_z^2}{2} + \frac{\sigma_z^2}{2}w^2} \exp\left(\frac{\sigma^4 K^2}{4(\sigma^2 - \frac{\sigma_z^2}{2} + \frac{\sigma_z^2}{2}w^2)}\right). \tag{3.15}$$

The matrix element $V_{\Phi k \Phi k'}$ can be thus explicitly written as

$$V_{\Phi k \Phi k'} = \frac{e^2\sigma^2}{2\pi^2\epsilon\epsilon_0 S} e^{-\frac{\sigma^2}{2}(k^2+k'^2)} \left(\frac{J_1}{2} - \frac{J_2}{\sqrt{\pi}}\right), \tag{3.16}$$

with J_1 and J_2 given by Eqs. (3.14) and (3.15), respectively. In order to simplify the notation in further calculation the following notation, which indicates explicit dependence on $\boldsymbol{k}$ and $\boldsymbol{k}'$, will be used:

$$V_{\Phi k \Phi k'} = V\left(k^2 + k'^2, (\boldsymbol{k} + \boldsymbol{k}')^2\right).$$

Having calculated the matrix element, one can now calculate the expression for the transition probability, given by Eq. (3.11). First, the summation is changed into integration, according to: $\sum_{\boldsymbol{k}} \to \frac{S}{(2\pi)^2}\int d^2k$. Then, Dirac delta is transformed, $\delta(E_k - E_{k'}) = 2m\delta(k^2 - k'^2)/\hbar^2$. Finally, introducing the new constant $C = mS/\pi\hbar^3$ one obtains

$$P_{(\boldsymbol{k}'\downarrow,\Phi\uparrow)\to(\boldsymbol{k}\uparrow,\Phi\downarrow)} = C\int d^2k \left|V\left(k^2 + k'^2, (\boldsymbol{k} + \boldsymbol{k}')^2\right)\right|^2 \delta\left(k^2 - k'^2\right). \tag{3.17}$$

It is convenient to introduce polar coordinates such that the x axis is determined by $\boldsymbol{k}' = k'(1,0,0)$ and $\tilde{\boldsymbol{k}} = k'(\cos\phi, \sin\phi, 0)$ is any wave vector with the same length as $\boldsymbol{k}'$ (due to the Dirac delta only vectors of the same length will give contribution to the integral). Then,

$$(\boldsymbol{k}+\boldsymbol{k}')^2 = 4k'^2\cos^2\frac{\phi}{2},$$

and Eq. (3.17) can be written as

$$P_{(\boldsymbol{k}'\downarrow,\Phi\uparrow)\to(\boldsymbol{k}\uparrow,\Phi\downarrow)} = C\int_0^{2\pi} d\phi \int_0^{\infty} kdk \left|V\left(\frac{\phi}{2}, k'^2\right)\right|^2 \delta\left(k^2 - k'^2\right).$$

Finally, changing the integration variable, $x = k^2$, and indicating the only explicit dependence of transition probability on the length of the initial wave vector, $P_{(\boldsymbol{k}'\downarrow,\Phi\uparrow)\to(\boldsymbol{k}\uparrow,\Phi\downarrow)} = P\left(k'^2\right)$, one arrives at the expression

$$P\left(k'^2\right) = \frac{C}{2}\int_0^{2\pi} d\phi \left|V\left(\frac{\phi}{2}, k'^2\right)\right|^2. \tag{3.18}$$

In order to obtain total transition probability $\mathcal{P}$ one has to sum the transition probability $P(k'^2)$ over all the initial states with the factor $f(k'^2)\cdot(1-f(k'^2))$ [where $f(k'^2)$ is the Fermi-Dirac distribution function given by Eq. (3.2)] to make sure that the initial state is occupied and the final state is empty. The summation is, as usual, changed into integration in polar coordinates (due to isotropy, the angular integral gives only 2π) and the integration variable $x = k^2$ is introduced. Then, the expression for the total transition probability is given by

$$\mathcal{P} = \frac{S}{4\pi}\int_0^{\infty} dx P(x) f(x)\left(1 - f(x)\right), \tag{3.19}$$

and Eqs. (3.18), (3.16), (3.14), (3.15), in terms of new variables x and ϕ, are given by

$$P(x) = \frac{mS}{2\pi\hbar^3}\int_0^{2\pi} d\phi \left|V\left(\frac{\phi}{2}, x\right)\right|^2, \tag{3.20}$$

$$V\left(\frac{\phi}{2}, k'^2\right) = \frac{e^2\sigma^2}{2\pi^2\epsilon\epsilon_0 S} e^{-\sigma^2 x}\left(\frac{J_1}{2} - \frac{J_2}{\sqrt{\pi}}\right), \tag{3.21}$$

$$J_1 = \frac{\pi^{\frac{3}{2}}}{2\sqrt{\sigma^2 - \frac{\sigma_z^2}{2}}}\exp\left(\frac{\sigma^4 x\cos^2\frac{\phi}{2}}{2\left(\sigma^2 - \frac{\sigma_z^2}{2}\right)}\right) I_0\left(\frac{\sigma^4 x\cos^2\frac{\phi}{2}}{2\left(\sigma^2 - \frac{\sigma_z^2}{2}\right)}\right), \tag{3.22}$$

$$J_2 = \frac{\sqrt{\pi}\sigma_z}{\sqrt{2}}\int_0^1 dw \frac{1}{\sigma^2 - \frac{\sigma_z^2}{2} + \frac{\sigma_z^2}{2}w^2}\exp\left(\frac{\sigma^4 x\cos^2\frac{\phi}{2}}{\left(\sigma^2 - \frac{\sigma_z^2}{2} + \frac{\sigma_z^2}{2}w^2\right)}\right). \tag{3.23}$$

The resulting dephasing rates are presented and discussed in Sec. 4.3.

Chapter 4

Results

In this chapter, all the results of the developed theoretical models are presented and compared with the experimental measurements (provided by the Regensburg group). First, the solutions for the spin dynamics for various experimental conditions and the resulting TRKR signals are given. Then, the modeled RSA signals, also for different excitation conditions and magnetic field configurations, are presented. In both cases, fittings to the experimental data are also shown and the parameters of spin dynamics are extracted. Finally, the results concerning the microscopic model of decoherence, i.e. the temperature dependencies of the hole spin lifetimes, are presented. Results concerning the TRKR and RSA experiments, apart from the ones performed in tilted fields, have been published in Ref. [15].

4.1 TRKR experiment

In general, to calculate the TRKR signal one has to solve the set of differential equations 2.23-2.25 (in this work this was done by the use of Laplace transform technique) and, using obtained solutions for Σ_{h} and Σ_{t} [the former being given by Eq. (2.22)], find the TRKR response as given by Eq. (2.43). The initial values of the dynamical variables given by the vector $\boldsymbol{S}_2$ are responsible for different excitation conditions (through their dependence on pump pulse and fast decoherence) and can be explicetely written as:

$$\Sigma_{\mathrm{h}}(0) = e^{-u}\left((1-2|F(\Delta)|^2)p\cos\phi - 2|F(\Delta)|^2 - p\cos\phi\right) + p\cos\phi, \tag{4.1}$$

$$X_{\mathrm{h}}(0) = e^{-u/2-w}\left((1-2|F(\Delta)|^2)p\sin\phi - p\sin\phi\right) + p\sin\phi, \tag{4.2}$$

$$Y_{\mathrm{h}}(0) = e^{-u/2-w}2M(\Delta)p\sin\phi, \tag{4.3}$$

$$\Sigma_{\mathrm{t}}(0) = 2|F(\Delta)|^2 p\cos\phi + 2|F(\Delta)|^2, \tag{4.4}$$

$$N_{\mathrm{t}}(0) = \Sigma_{\mathrm{t}}(0). \tag{4.5}$$

The general solution, for arbitrary magnetic field, is a rather complicated expression. Therefore, to get the formulas with clear physical interpretation, three special cases were considered.

No magnetic field

In the case of no magnetic field, i.e. for $\omega_{\mathrm{h}} = \omega_{\mathrm{t}} = 0$, the equations of motion for the dynamical variables are significantly simplified and the expressions for the trion and hole polarizations (note that without the magnetic field equilibrium hole spin polarization vanishes) are given by

$$\begin{aligned} \Sigma_{\mathrm{t}}(t) &= \widetilde{\Sigma}_{\mathrm{t}}(t) = \Sigma_{\mathrm{t}}(0)e^{-\gamma_1 t}, \\ \Sigma_{\mathrm{h}}(t) &= \widetilde{\Sigma}_{\mathrm{h}}(t) = e^{-\kappa t}\Sigma_{\mathrm{h}}(0) + \eta\left(e^{-\kappa t} - e^{-\gamma_1 t}\right)\Sigma_{\mathrm{t}}(0), \end{aligned}$$

where $\kappa = \kappa_x + \kappa_{x0}$ and $\eta = \gamma_1/(\gamma_1 - \kappa)$. The initial values are also simplified,

$$\begin{aligned} \Sigma_{\mathrm{t}}(0) &= 2|F(\Delta)|^2, \\ \Sigma_{\mathrm{h}}(0) &= -e^{-u}2|F(\Delta)|^2 = -e^{-u}\Sigma_{\mathrm{t}}(0). \end{aligned}$$

Using Eq. (2.43), the TRKR signal is

$$\mathrm{TRKR} = \Sigma_{\mathrm{t}}(0)\left(e^{-\gamma_1 t}(\eta+1) - e^{-\kappa t}(\eta - e^{-u})\right). \tag{4.6}$$

The physical interpretation of this formula is as follows. Under resonant excitation (i.e. $\Delta = 0$, $u = 0$) and in the absence of a magnetic field, optically oriented electron and hole spins retain their orientation during the photocarrier lifetime. During recombination of electrons and holes with matching spins (according to the optical selection rules), the spin polarization is completely removed from the sample. Therefore, the TRKR signal nearly-monoexponentialy decays from the initial value (equal to $4|F(0)|^2$) to zero on the timescale of the trion lifetime, as no hole spin polarization is transferred to the resident holes. However, under nonresonant excitation, the hole spin polarization is rapidly (modeled as instantaneously) shrinked by the factor e^{-u} (the probable mechanism behind this effect was described in sec. 2.3), in contrast to the electron spins, which retain their orientation. Then, during recombination, spin-polarized electrons remove holes with matching spin from the partly depolarized hole system, leaving an excess of holes oriented opposite to the optically created hole spin orientation (therefore, this orientation will be refered to as *negative*). This results in the increase of time during which the spin polarization is observed, as it is no longer limited by the trion lifetime but rather by the hole SDT. The schematic picture of the mechanism described here (which will be reffered to as decoherence-induced mechanism) is presented in Fig. 4.1.

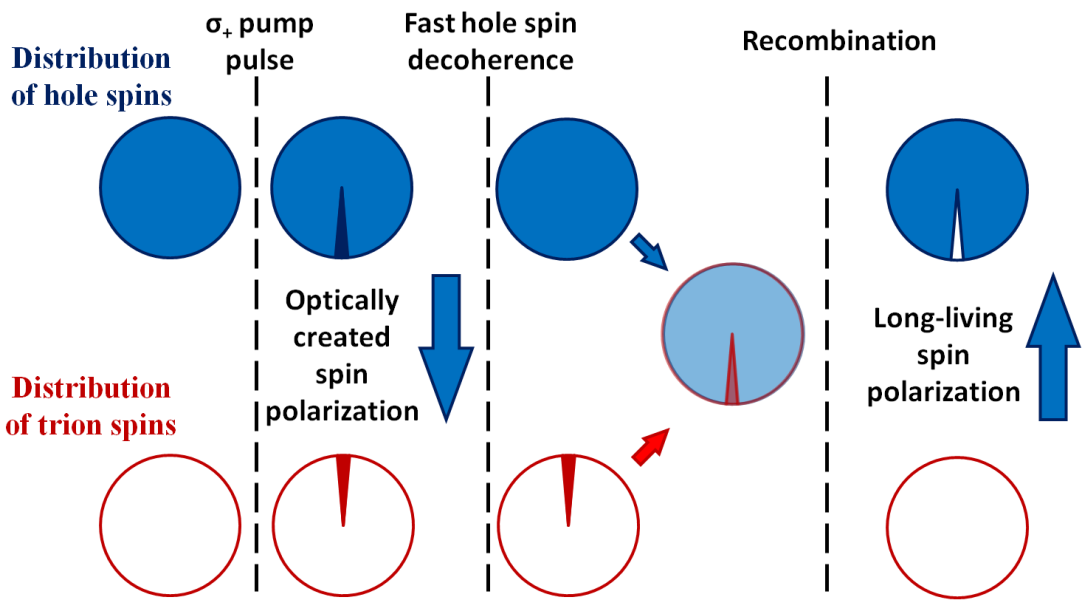

Figure 4.1: Schematic picture representing decoherence-assisted initialization of resident hole spin polarization (long-living hole spin polarization). Distribution of hole (trion) spin orientation is presented on the circles, with blue (red) color corresponding to hole (trion) spins (darker colors correspond to bigger values, white means 0).

Two kinds of TRKR measurements at zero magnetic field were performed by the Regensburg group. First, the Kerr response for non-resonant excitation conditions was investigated (see Fig. 4.2), where the excitation wavelength was tuned from near-resonant ($\lambda = 743$ nm) to 7 meV off-resonance (739.8 nm). Then, the power-dependent series of measurements were performed, with power varying up to three orders of magnitude (see Fig. 4.3). In the first case, the temperature was set to $T = 15$ K, in the second to $T = 10$ K. Experimental traces for both measurements are well reproduced by Eq. (4.6) [red, solid lines in Figs. 4.2 and 4.3 correspond to the fits according to Eq. (4.6)] in the whole time range, except for the first few picoseconds after excitation, in which the rapid initial dephasing of the holes occurs that is not modeled in a time-resolved manner in the theory. Using the least-squares fit algorithm, all the parameters were extracted: the ratio of the hole and trion spin polarizations after the initial dephasing, $\Sigma_{\mathrm{h}}(0)/\Sigma_{\mathrm{t}}(0) = -e^{-u}$, trion recombination rate γ_1 and the hole decoherence rate κ (see Figs. 4.2 and 4.3 for the results). As the values of γ_1 and κ remain nearly constant throughout the investigated detuning and power range, the photocarrier and hole spin dynamics are not strongly influenced by the fast initial decoherence.

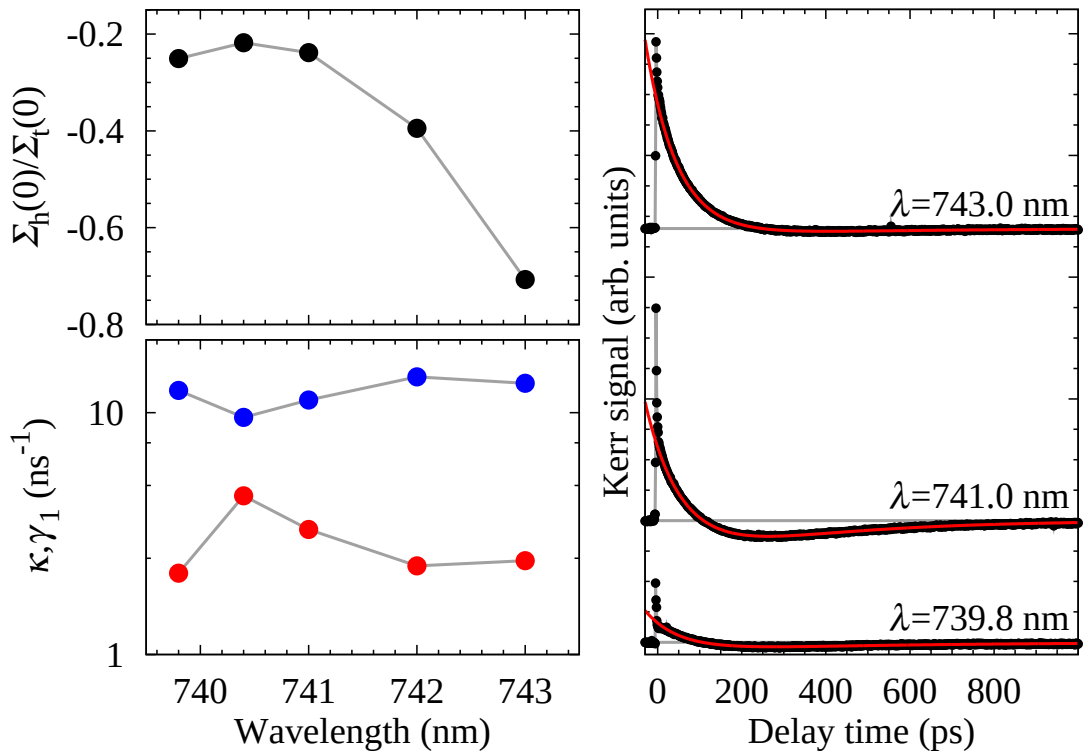

Figure 4.2: Experimental (black dots) and modeled (red line) Kerr signal in the absence of magnetic field for different excitation wavelengths (right), along with the evolution parameters extracted from the fitting procedure: hole-to-trion spin polarization after fast decoherence, $\Sigma_h(0)/\Sigma_t(0) = -e^{-u}$ (top left) and decay rates κ, γ_1 (bottom left, blue and red dots, respectively). Experimental data source: Ref. [15].

Voigt configuration

For magnetic fields applied in the sample plane (Voigt configuration, $\phi = \pi/2$, $\theta = \pi/2$), another useful approximation, which allows for great simplification of the formulas, is made. Namely, taking into account that the focus of the investigation is on the long hole SDT regime, the hole decoherence rates are assumed to be smaller than precession frequencies ω_t, ω_h (which means that spins live at least for few precession periods) and radiative decay rate γ_1. However, for very small precession frequencies (in the case of weak magnetic field), this approximation is not valid. Still, it is plausible for most cases of TRKR experiments, due to relatively strong magnetic fields applied. In the case of a RSA experiment (where magnetic field varies from 0 to some fixed value), which will be discussed later, this assumption is not valid and will not be used. With the use of this approximation, the expressions for the trion and hole polarizations are

$$\Sigma_t(t) = \Sigma_t(0)e^{-\gamma_1 t}\cos\omega_t t, \tag{4.7}$$

$$\widetilde{\Sigma}_h(t) = Ae^{-(\gamma_1+i\omega_t)t} + Be^{-(\kappa+i\omega_h)t} + \text{c.c.}, \tag{4.8}$$

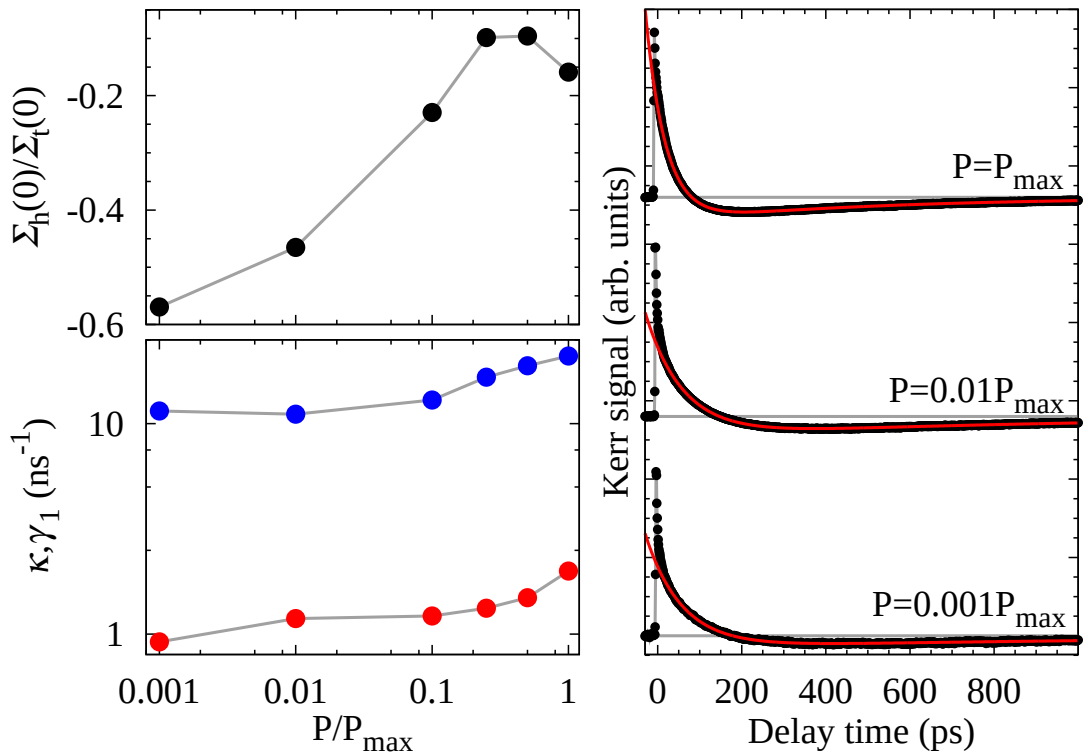

Figure 4.3: Experimental (black dots) and modeled (red line) Kerr signal in the absence of magnetic field for different excitation powers (right), along with the evolution parameters extracted from the fitting procedure: hole-to-trion spin polarization after fast decoherence, $\Sigma_\mathrm{h}(0)/\Sigma_\mathrm{t}(0) = -e^{-u}$ (top left) and decay rates κ, γ_1 (bottom left, blue and red dots, respectively). Experimental data source: Ref. [15].

where $\kappa = \kappa_{x0} + (\kappa_x + \kappa_z)/2$ and the prefactors are:

$$A = -\frac{1}{2}\frac{\gamma_1(\gamma_1 + i\omega_\mathrm{t})}{\omega_\mathrm{h}^2 + (\gamma_1 + i\omega_\mathrm{t})^2}\Sigma_\mathrm{t}(0), \tag{4.9}$$

$$B = \frac{1}{2}\frac{\gamma_1(\gamma_1 - i\omega_\mathrm{h})}{\omega_\mathrm{t}^2 + (\gamma_1 - i\omega_\mathrm{h})^2}\Sigma_\mathrm{t}(0) + \frac{1}{2}\widetilde{\Sigma}_\mathrm{h}(0) + \frac{i}{2}Y_\mathrm{h}(0). \tag{4.10}$$

The corresponding TRKR signal is

$$\mathrm{TRKR} = \left(\frac{\Sigma_\mathrm{t}(0)}{2} - A\right) e^{-(\gamma_1 + i\omega_\mathrm{t})t} - Be^{-(\kappa + i\omega_\mathrm{h})t} + \mathrm{c.c.} \tag{4.11}$$

The physical interpretation of this formula will now be discussed. First of all, as can be seen from Eq. (4.8), the hole polarization is composed of two components. The first one (with coefficient A and its complex conjugate), which will be denoted by $\Sigma_\mathrm{h}^{(\mathrm{short})}(t)$, depends on the parameters of the trion dynamics (ω_t and γ_1) and originates from the following mechanism. Trions recombine with holes with matching spins during precession at different times. Therefore, during recombination, hole spins of different orientations

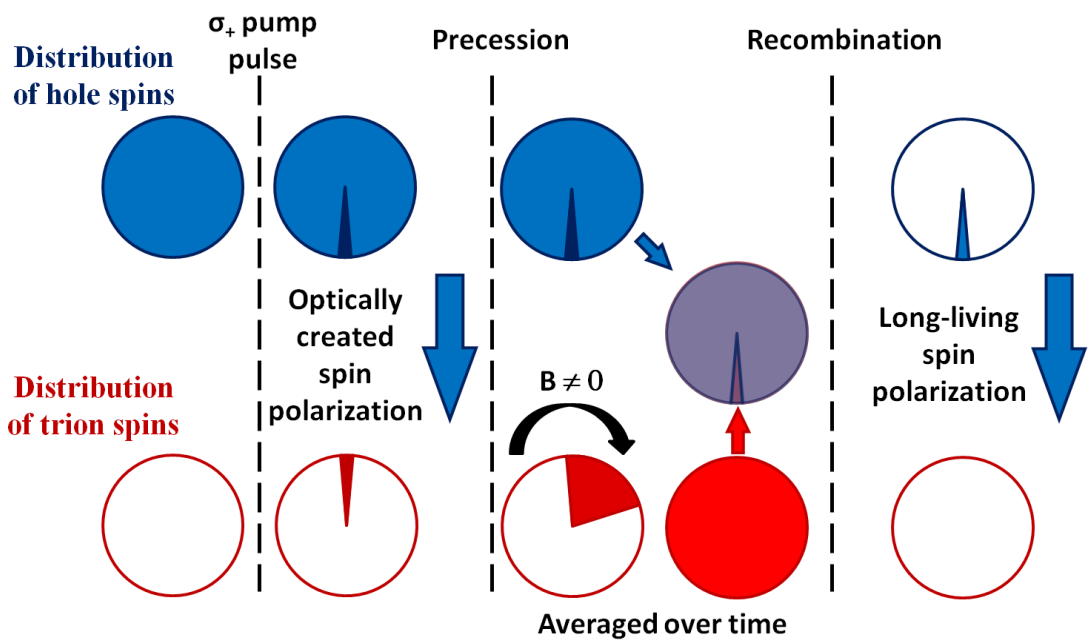

Figure 4.4: Schematic picture representing precession-induced initialization of resident hole spin polarization (long-living hole spin polarization). Distribution of hole (trion) spin orientation is presented on the circles, with blue (red) color corresponding to hole (trion) spins (darker colors correspond to bigger values, white means 0).

are removed, not only the optically oriented ones (which, of course, affects the hole spin polarization the same way as the trion spin polarization: with frequency ω_{t} and decay rate γ_1). In Fig. 4.4, a schematic picture of this mechanism is shown for the idealized situation with $\omega_{\mathrm{t}} \to \infty$, for which the removed holes are evenly distributed over all spin orientations. In a realistic case, holes with different spin orientations will be removed with different rates and the obtained hole polarization should, in general, depend on both the frequencies and the recombination rate, which is reflected by Eq. (4.9). The second component of the hole spin polarization (with coefficient B and its complex conjugate), which will be denoted by $\Sigma_{\mathrm{h}}^{(\mathrm{long})}(t)$, describes the long-living evolution (with decay rate κ and precession frequency ω_{h}) of the spin polarization, that is not removed during recombination. Both hole spin polarization components, along with the trion spin polarization, form the TRKR signal that can also be divided into 2 parts: short-living, precessing with the trion Larmor frequency, and long-living, precessing with the hole Larmor frequency [Eq. (4.11)]. An exemplary TRKR signal for resonant pumping, divided into its components, is shown in Fig. 4.5.

As the short-living part is not of great interest, we will now focus on the $\Sigma_{\mathrm{h}}^{(\mathrm{long})}$ component. There are two sources of the long-living spin polarization: precession-induced mechanism, described in this subsection, and decoherence-induced mechanism, described

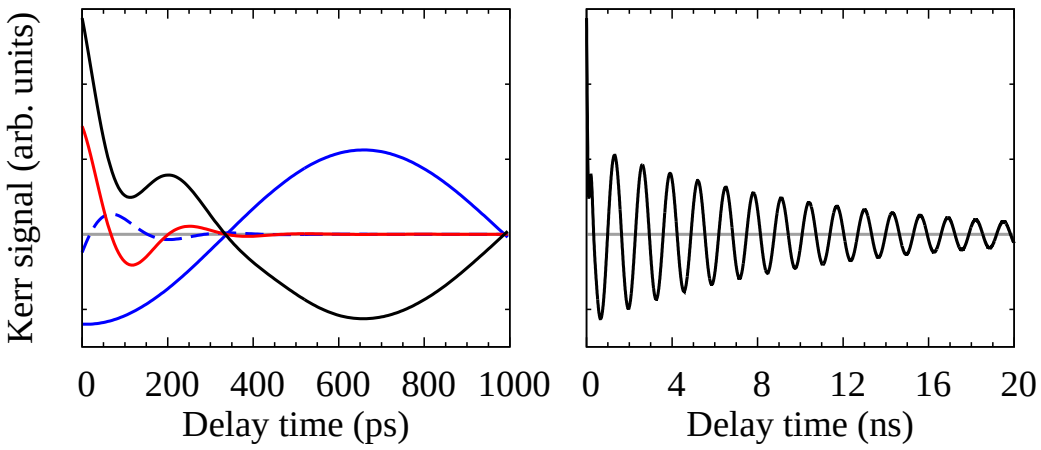

Figure 4.5: Simulated TRKR signal (black, solid lines) on the short (left) and long (right) time scales for resonant pumping (no fast decoherence, $u = w = 0$). Additionaly, on the short time scale, signal components are drawn: long-living hole spin polarization $\Sigma_{\mathrm{h}}^{(\mathrm{long})}$ (blue, solid line), short-living hole spin polarization $\Sigma_{\mathrm{h}}^{(\mathrm{short})}$ (blue, dashed line) and trion spin polarization Σ_{t} (red, solid line). Parameters used for modelling: $\gamma_1 = 0.1$ ns^{-1}, $\kappa = 10$ ns^{-1}, hole in-plane g-factor $g_\perp = 0.055$, trion (electron) g-factor $g_{\mathrm{t}} = 0.266$ and magnetic field $B = 1$ T.

in the last subsection. As can easily be seen, by comparing Figs. 4.4 and 4.1, the two mechanisms produce hole spin polarization of opposite signs: the first one is parallel to the optical orientation, the second one is antiparallel. Therefore, combining these two mechansims allows one to control the phase of the long-living part of polarization, $\Sigma_{\mathrm{h}}^{(\mathrm{long})}$, at a given time. To show this, $\Sigma_{\mathrm{h}}^{(\mathrm{long})}$ is written in the form

$$\Sigma_{\mathrm{h}}^{(\mathrm{long})}(t) = e^{-\kappa t}\left[(a - e^{-u})\cos(\omega_{\mathrm{h}} t) + b\sin(\omega_{\mathrm{h}} t)\right]\Sigma_{\mathrm{t}}(0), \tag{4.12}$$

where

$$a = \Re\left(\frac{\gamma_1(\gamma_1 - i\omega_{\mathrm{h}})}{\omega_{\mathrm{t}}^2 + (\gamma_1 - i\omega_{\mathrm{h}})^2}\right), \quad 0 < a < 1,$$

$$b = \Im\left(\frac{\gamma_1(\gamma_1 - i\omega_{\mathrm{h}})}{\omega_{\mathrm{t}}^2 + (\gamma_1 - i\omega_{\mathrm{h}})^2}\right), \quad 0 < b < 1,$$

and the relation $\Sigma_{\mathrm{h}}(0) = -e^{-u}\Sigma_{\mathrm{t}}(0)$ [Eq. (4.1)] was used, together with putting $Y_{\mathrm{h}}(0)$ to 0, as it is negligibly small, both due to dependence on p and $M(\Delta)$. Now, the Eq. (4.12), can be rewritten in the form

$$\Sigma_{\mathrm{h}}^{(\mathrm{long})}(t) = \frac{a - e^{-u}}{\cos\alpha}\cos(\omega_{\mathrm{h}} t + \alpha)e^{-\kappa t}\Sigma_{\mathrm{t}}(0), \tag{4.13}$$

where

$$\alpha = \arctan\left(\frac{b}{e^{-u} - a}\right). \tag{4.14}$$

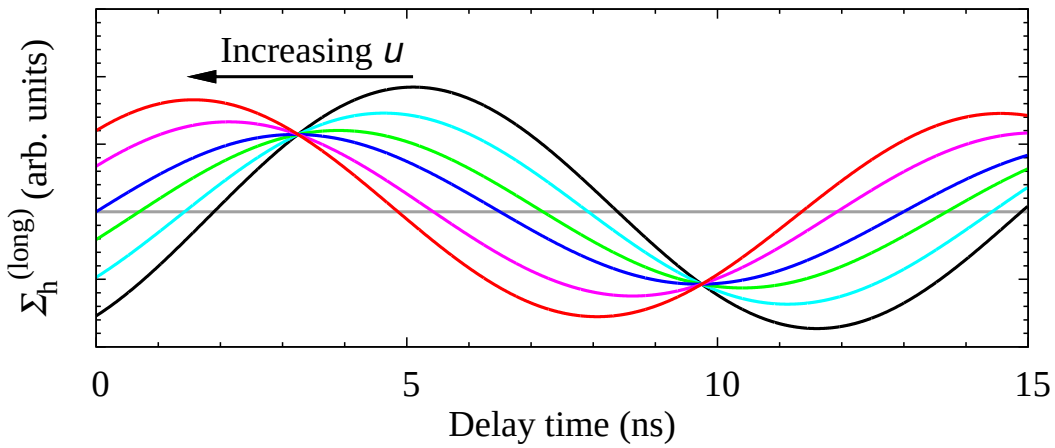

Figure 4.6: Simulated long-living hole spin polarization components of TRKR signals for different fast decoherence parameters u. The phase of the signal is moving from α_0 for $u = 0$, i.e. no detuning (black line), through $\alpha = \pi/2$ for $u = -\ln a$ and further (red line corresponds to biggest u). Parameters used in the modelling: $\gamma_1 = 0.1$ ns^{-1}, $\kappa = 100$ ns^{-1}, hole in-plane g-factor $g_\perp = 0.055$, trion (electron) g-factor $g_t = 0.266$ and magnetic field $B = 0.1$ T.

By changing the fast decoherence parameter u from 0 to infinity one can control the phase shift α. The discontinuity of the arctan function (when going through $a = e^{-u}$) is exactly cancelled by the sign change of the factor in front of the expression 4.13. One therefore obtains:

$$\Sigma_h^{(long)}(t) = -\frac{|a - e^{-u}|}{\cos\alpha}\cos(\omega_h t + \alpha)e^{-\kappa t}\Sigma_t(0),$$

with α varying from $\alpha_0 = \arctan(b/(1-a))$ (for $u = 0$), through $\pi/2$ (for $a = \exp(-u)$) to $\alpha_\infty = \pi/2 + \arctan(b/a)$. Fig. 4.6 shows the effect of phase shift for different fast decoherence parameters u. To control α one can of course also change a or b, which effectively means changing the magnetic field (which affects Larmor frequencies ω_t and ω_h, that a and b depend on). However, this would also change the frequency of oscillations and the effect of phase shift would not be clearly seen in the TRKR signal. Nevertheless, if one is interested in the phase of the signal at time $t = 0$, which is the case in the RSA experiment, then it is possible to change α controlling both u and B. This control and its effect will be discussed in details in the subsection concerning the RSA signal.

Tilted magnetic field

Here, the same approximation as in the previous subsection is used, i.e., the hole decoherence rates are assumed to be smaller than the other dynamical parameters of the system.

Then, the solutions for trion and hole spin polarizations are given by

$$\Sigma_{\rm t}(t) = \Sigma_{\rm t} t(0) e^{-\gamma_1 t}\left(\cos^2\theta + \sin^2\theta\cos\omega_{\rm t} t\right) \tag{4.15}$$

$$\begin{aligned}\widetilde{\Sigma}_{\rm h}(t) =& A_1 e^{-\gamma_1 t} + A_2 e^{-(\gamma_1 + i\omega_{\rm t})t} + B_1 e^{-(\kappa_{1\perp}\sin^2\phi + \kappa_{1\parallel}\cos^2\phi)t} \\ &+ B_2 e^{-(\kappa_{2\perp}\sin^2\phi + \kappa_{2\parallel}\cos^2\phi + i\omega_{\rm h})t} + \text{c.c.},\end{aligned} \tag{4.16}$$

where the coefficients are

$$A_1 = -\frac{1}{2}\frac{\omega_{\rm h}^2\cos^2\phi + \gamma_1^2}{\omega_{\rm h}^2 + \gamma_1^2}\cos^2\theta\Sigma_{\rm t}(0), \tag{4.17}$$

$$A_2 = -\frac{1}{2}\frac{\gamma_1}{\gamma_1 + i\omega_{\rm t}}\frac{\omega_{\rm h}^2\cos^2\phi + (\gamma_1 + i\omega_{\rm t})^2}{\omega_{\rm h}^2 + (\gamma_1 + i\omega_{\rm t})^2}\sin^2\theta\Sigma_{\rm t}(0), \tag{4.18}$$

$$B_1 = \frac{1}{2}\frac{\omega_{\rm t}^2\cos^2\theta + \gamma_1^2}{\omega_{\rm t}^2 + \gamma_1^2}\cos^2\phi\Sigma_{\rm t}(0) + \frac{1}{2}\cos^2\phi\widetilde{\Sigma}_{\rm h}(0) + \frac{1}{4}\sin 2\phi\widetilde{X}_{\rm h}(0), \tag{4.19}$$

$$\begin{aligned}B_2 =& \frac{1}{2}\frac{\gamma_1}{\gamma_1 - i\omega_{\rm h}}\frac{\omega_{\rm t}^2\cos^2\theta + (\gamma_1 - i\omega_{\rm h})^2}{\omega_{\rm t}^2 + (\gamma_1 - i\omega_{\rm h})^2}\sin^2\phi\Sigma_{\rm t}(0) + \frac{1}{2}\sin^2\phi\widetilde{\Sigma}_{\rm h}(0) \\ &-\frac{1}{4}\sin 2\phi\widetilde{X}_{\rm h}(0) + \frac{i}{2}\sin\phi Y_{\rm h}(0),\end{aligned} \tag{4.20}$$

and the new dephasing rates are defined as

$$\begin{aligned}\kappa_{1\perp} &= \kappa_x + \kappa_z, \\ \kappa_{1\parallel} &= 2\kappa_x, \\ \kappa_{2\perp} &= \frac{\kappa_x + \kappa_z}{2} + \kappa_{x0}, \\ \kappa_{2\parallel} &= \kappa_x + \kappa_{z0}.\end{aligned}$$

The corresponding expression for the TRKR signal is given by

$$\begin{aligned}\text{TRKR} =& \left[\frac{\Sigma_{\rm t} t(0)}{2}\left(\cos^2\theta + \sin^2\theta\cos\omega_{\rm t} t\right) - A_1\right] e^{-\gamma_1 t} + A_2 e^{-(\gamma_1 + i\omega_{\rm t})t} \\ &+ B_1 e^{-(\kappa_{1\perp}\sin^2\phi + \kappa_{1\parallel}\cos^2\phi)t} + B_2 e^{-(\kappa_{2\perp}\sin^2\phi + \kappa_{2\parallel}\cos^2\phi + i\omega_{\rm h})t} + \text{c.c.}\end{aligned} \tag{4.21}$$

The physical interpretation of Eq. (4.21) will now be given. First of all, since in a tilted magnetic field, the quantization axis for holes (trions) forms the angle ϕ (θ) with the structure axis a non-zero component of the optically oriented hole (trion) spin polarization along the quantization axis exists. Therefore, the spin polarization should split into two parts: non-precessing along the quantization axis (which coincides with magnetic field axis for electrons but, due to anisotropic hole g-factor, does not for holes) and precessing, perpendicular to this axis. This is reflected in the equations: the precessing parts of both trion and hole polarizations (coefficients A_2 and B_2) are proportional to $\cos^2\theta$ or $\cos^2\phi$ and the non-precessing components (coefficients A_1 and B_1) are proportional to $\sin^2\theta$ or $\sin^2\phi$. Secondly, the same decomposition of the hole spin polarization and of the whole TRKR

signal as for the Voigt configuration can be made. Namely, short-living component $\Sigma_{\mathrm{h}}^{(\mathrm{short})}$ (corresponding coefficients: A_1 and A_2) and long-living component $\Sigma_{\mathrm{h}}^{(\mathrm{long})}$ (corresponding coefficients: B_1 and B_2) exist, due to the same mechanism as described in the previous section. Finally, the the new dephasing rates can be connected with the spin relaxation time T_1 and the spin dephasing time T_2 in the following way:

$$T_1(\phi) = \left(\frac{\kappa_{1\perp}+\kappa_{1\parallel}}{2}+\frac{\kappa_{1\parallel}-\kappa_{1\perp}}{2}\cos 2\phi\right)^{-1}, \tag{4.22}$$

$$T_2(\phi) = \left(\frac{\kappa_{2\perp}+\kappa_{2\parallel}}{2}+\frac{\kappa_{2\parallel}-\kappa_{2\perp}}{2}\cos 2\phi\right)^{-1}. \tag{4.23}$$

Due to the anisotropy of the hole g-factor, the tilting of magnetic field increases Zeeman frequncy for holes, ω_{h}. This results in the change of the dephasing parameters, since they depend on the spectral densities of the reservoir at the frequency ω_{h} [see Eq. (2.26)]. Therefore, the TRKR measurements in tilted magnetic fields were performed by the Regensburg group in the following way. Simultaneously with the increase of magnetic field tilt angle, its magnitude was decreased, in order to keep the hole precession frequency ω_{h} constant. In this way, the dephasing rates were kept constant, which allowed us to use the same fitting parameters for different tilt angles. Three series of experimental measurements in tilted magnetic fields were performed, for three different hole precession frequencies. These corresponded to three values of the in-plane (zero tilt angle) magnetic field 2 T, 3.5 T, 5 T and precession periods ($\tau = 2\pi/\omega_{\mathrm{h}}$) $\tau_1 \sim 500$ ps, $\tau_2 \sim 300$ ps and $\tau_3 \sim 200$ ps, respectively. In each series, the tilt angle was changed from 0° ($\theta = \phi = \pi/2$) to 85° and the temperature was set to 1.2 K.

The fitting procedure consisted of three steps. First, the fitting algorithm for the zero tilt angle ($\theta = \phi = \pi/2$) was applied because in the Voigt geometry the dependences on $g_\parallel$, $\kappa_{1\perp}$, $\kappa_{1\parallel}$ and $\kappa_{2\parallel}$ vanish. From this fitting, $g_\perp$ and $\kappa_{2\perp}$ were extracted and used in the subsequent fittings as constant parameters. Next, three tilt angles were chosen and a simultaneous fit to all three curves was made, in order to obtain $g_\parallel$, $\kappa_{1\perp}$, $\kappa_{1\parallel}$ and $\kappa_{2\parallel}$. In all fittings, $\kappa_{1\perp}$ was found to be at least 3 orders of magnitude smaller than other decoherence rates, so it was set to 0 (in order to decrease the number of fitting parameters and increase the precision of the fitting). Finally, all the parameters were set constant and the remaining curves were fitted, with some freedom left for the angle, i.e. the angle was allowed to differ by maximum 0.15° (this is justified by the fact that experimental setting of, e.g., 87° may have actually been 87.1° or 86.9°). At the end, sums of the squares of differences between measured and modeld signals were calculated and compared (for different triples of chosen tilt angles) to find the best fitting. Due to the similiar effect of inhomogeneous broadening and intrinisic decoherence on the TRKR signal (gaussian and exponential decay of the signal, respectively), the fitting procedure

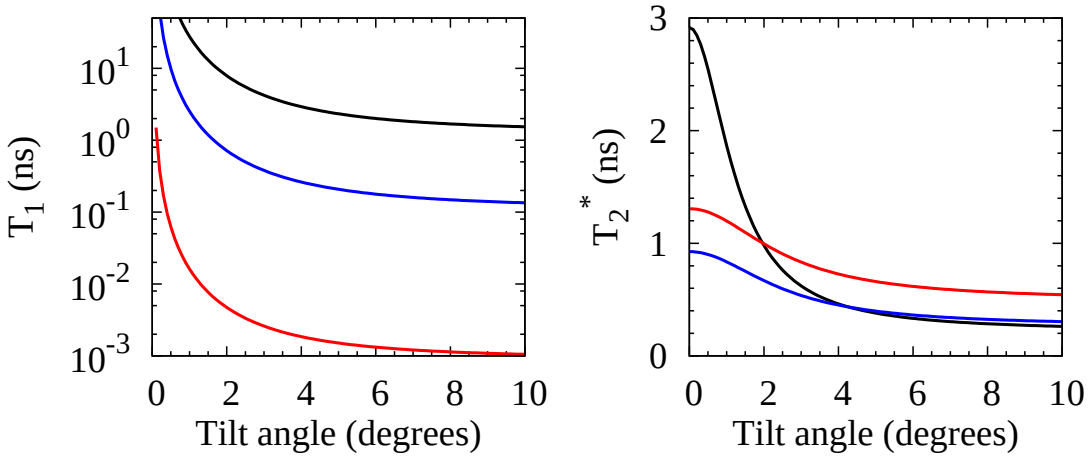

Figure 4.7: Effective spin relaxation and dephasing times, T_1 and T_2^*, as a function of the tilt angle for different hole precession periods: τ_1 (black), τ_2 (red) and τ_3 (blue).

could not distinguish between the two mechanims on such a short time scale (all the decay effects were attributed to the intrinisic decoherence, leaving the spread of hole g-factors equal to 0). Therefore, the inhomogenous broadening of the g-factors was not included during modelling and the effective T_1 and T_2^* times were extracted, instead of T_1 and T_2.

The experimental traces and the corresponding fitted curves, for all three series of measurements, are shown in Fig. 4.8. Extracted parameters of the evolution are collected in the table 4.1 and the tilt angle dependencies of the effective spin relaxation and dephasing times, T_1 and T_2^*, for the three measured cases, are presented in Fig. 4.7. Note that T_2^* depends on both intrinisic time T_2 and the inhomogeneity of the hole g-factor, which can be different for the in-plane and out-of plane components. The most reliable results are the in-plane component of the hole g-factor, $g_\perp$, and the dephasing rate $\kappa_{2\perp}$, as for the Voigt geometry the fitting procedure is the least complex. As can be seen from table 4.1, with the increasing magnitude of the magnetic field (decreasing τ) $\kappa_{2\perp}$ increases, which is an expected behaviour due to the inhomogeneous broadening of the hole g-factors. Concerning the rest of the parameters, the ones extracted for $\tau = 300$ ps series seem to be unreliable. First of all, there is a big discrepancy between the out-of-plane component of the hole g-factor extracted for this series and the other two. Secondly, enormously large value of $\kappa_{1\parallel}$ suggests that the fitting procedure completely omitted the strictly decaying part of the TRKR signal (for such a big value, the decaying part goes to 0 very quickly). Therefore, for parameters $\kappa_{1\parallel}$, $\kappa_{2\parallel}$ and $g_\parallel$ only the results for $\tau = 200$ ps and $\tau = 500$ ps series may be considered as reliable. The value of the out-of-plane component of the hole g-factor was found to be over 12 times larger that the value of the in-plane component. Spin relaxation time T_1 was found to decrease with the increasing magnitude of the magnetic field (as $\kappa_{1\parallel}$ increased), while $\kappa_{2\parallel}$ seems to slightly decrease.

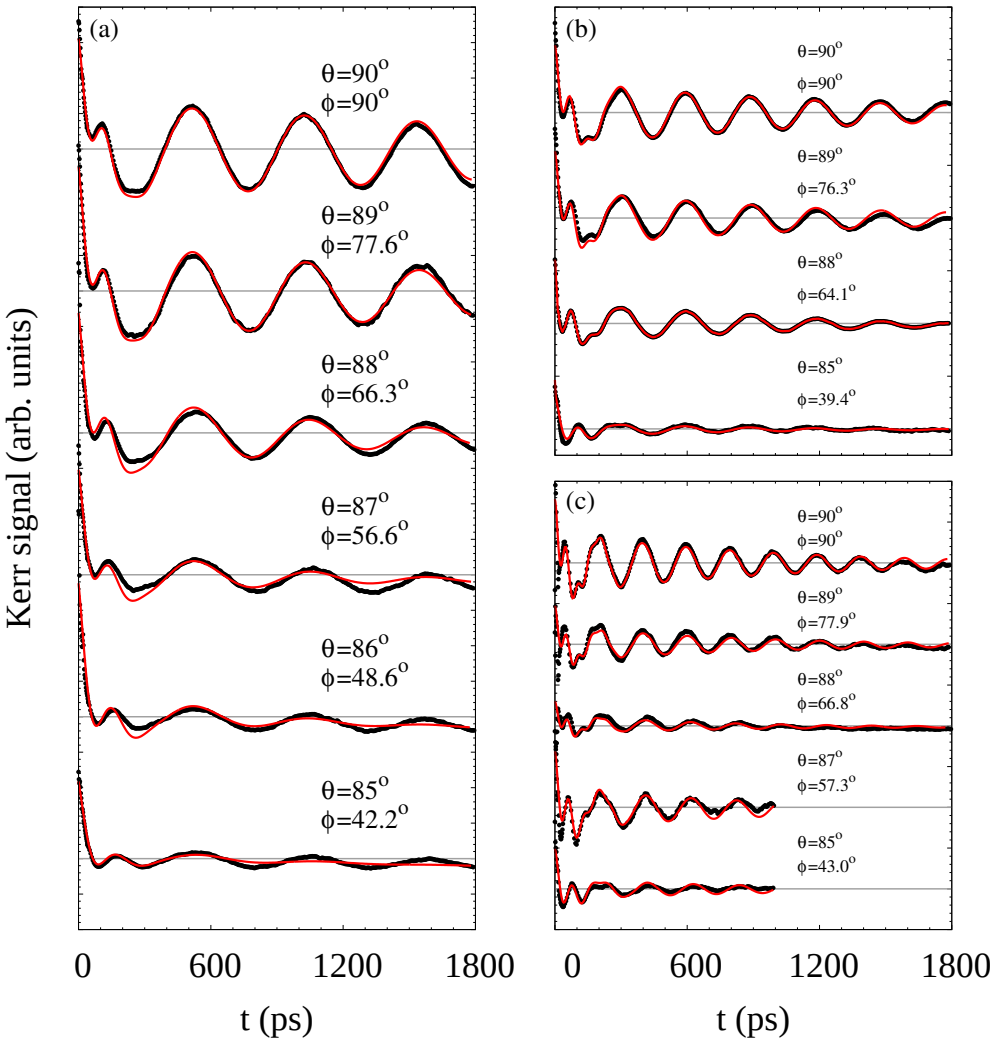

Figure 4.8: Experimental (black dots) and modeled (red lines) Kerr signals in tilted magnetic fields for different precession periods: (a) $\tau \sim 500$ ps, (b) $\tau \sim 300$ ps and (c) $\tau \sim 200$ ps. Experimental data source: unpublished data by the courtesy of Tobias Korn and Michael Kugler.

Table 4.1: Fitted parameters for the three different hole precession periods τ.

Precession period τ (ps)	$\kappa_{1\parallel}$ (ns^{-1})	$\kappa_{2\parallel}$ (ns^{-1})	$g_\parallel$	$\kappa_{1\perp}$ (ns^{-1})	$\kappa_{2\perp}$ (ns^{-1})	$g_\perp$
500	0.783	4.52	0.881	0	0.343	0.070
300	1110	2.02	0.960	0	0.765	0.069
200	9.01	3.76	0.883	0	1.08	0.072

4.2 RSA experiment

In order to obtain the expression for the RSA signal the stationary point of the three-step transformation, given by Eq. (2.28), has to be found for different magnetic fields. The general solution is even more complicated than the general solution for the TRKR signal, therefore two separate cases will be considered: RSA dependence on excitation conditions for fixed Voigt geometry (for which complete, analytical solution will be given) and RSA dependence on tilt angle of magnetic field (where only preliminary results will be presented). During calculations, the following approximations were made. First, the assumption of low-power pumping is maintained, so the field dependence only up to the second order is kept [there is no use of keeping higher-order corrections since some of them were already neglected, see Eq. (2.10)]. Secondly, since the RSA experiments are performed in the long SDT regime, it is assumed that all hole spin decoherence rates (all κs) are much smaller then the recombination rate γ_1. Note however, that the approximations from the previous section, $\kappa \ll \omega_\mathrm{t}$ and $\kappa \ll \omega_\mathrm{h}$, are not used, since they are obviously not correct for weak magnetic fields. Moreover, it is assumed that the intrinsic dephasing rates, κs, are constant in the relevant range of the magnetic field. This amounts to assuming that the spectral densities of the reservoir coupled to the hole spins are constant in the corresponding range of frequencies. Finally, because the laser repetition period t_r is of the order of tens of nanoseconds and the photocarrier lifetime is of the order of hundreds of picoseconds, only long-living part of the spin polarization is preserved, i.e., all the components with factor the $e^{-\gamma_1 t_\mathrm{r}}$ are put to 0. At the end, as mentioned in Sec. 2.5, in order to model the response from an inhomogeneous ensemble of hole spins, the obtained expression for the RSA signal is numerically averaged according to a Gaussian distribution of hole g-factors with the standard deviation Δg.

Different excitation conditions in Voigt geometry

In the Voigt geometry, the expression for the RSA signal has the form

$$\Delta\Sigma^{(\mathrm{RSA})} \sim f\frac{P}{Q}, \tag{4.24}$$

where

$$f = 1 - e^{-u} - \frac{\omega_\mathrm{t}^2}{\gamma_1^2 + \omega_\mathrm{t}^2}, \tag{4.25}$$

$$P = (i\tilde{\omega} + \kappa')e^{i\tilde{\omega}t_\mathrm{r}/2} - i\tilde{\omega}e^{-u/2-w-\kappa t_\mathrm{r}/2} - (\tilde{\omega} \to -\tilde{\omega}), \tag{4.26}$$

$$Q = e^{-u}P + \left[(i\tilde{\omega} - \kappa')e^{-u/2-w+i\tilde{\omega}t_\mathrm{r}/2} - i\tilde{\omega}e^{\kappa t_\mathrm{r}/2} - (\tilde{\omega} \to -\tilde{\omega})\right], \tag{4.27}$$

with $\kappa = \kappa_x + \kappa_z + 2\kappa_{x0}$, $\kappa' = \kappa_z - \kappa_x$, $\tilde{\omega} = 2\sqrt{\omega_\mathrm{h}^2 - \kappa'^2/4}$, and $(\tilde{\omega} \to -\tilde{\omega})$ representing additional terms, obtained from the preceding ones by changing the sign of $\tilde{\omega}$. In order to

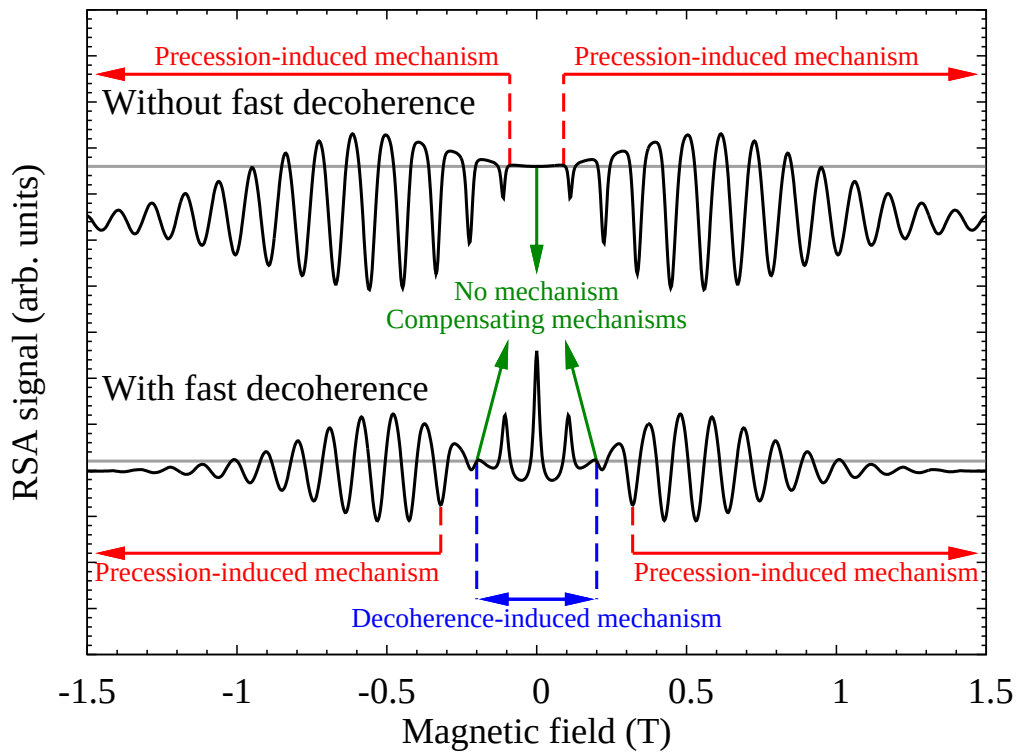

Figure 4.9: RSA traces obtained from Eq. (4.24) with (bottom) and without (top) fast hole spin decoherence. Different mechanisms responsible for the sign and value of the long-living spin polarization and, as a result, the RSA peaks are presented, together with the regions, where they dominate.

find the physical meaning of the dephasing rates κ, κ' the analysys of Eqs. (2.23)-(2.25) for Voigt geometry ($\phi = \theta = \pi/2$) in the limiting cases of $\omega_\mathrm{t} = 0$ and $\omega_\mathrm{t} \gg \kappa_\alpha, \kappa_{\alpha 0}$ (for $\alpha = x, z$) has to be made. In the first case, $\kappa_\alpha = \kappa_{\alpha 0}$ and the decoherence time for the spin polarization along the structure axis is $T_z^{(0)} = 1/2\kappa_{x0}$, while the decoherence time for the in-plane components of the spin polarization is $T_{xy}^{(0)} = 1/(\kappa_z + \kappa_{x0})$. In the second case, for sufficiently strong fields, the longitudinal (with respect to the field orientation) spin relaxation time is $T_1 = 1/(\kappa_z + \kappa_x)$ and the transverse relaxation (dephasing) time is $T_2 = 2/(\kappa_z + \kappa_x + 2\kappa_{x0}) = 2/\kappa$.

The physical interpretation of Eq. (4.24) will now be presented. The RSA signal arises from the interference of spin polarizations created in the sample by subsequent pump pulses. However, only long-living components of the spin-polarization can survive in between the pulses. Therefore, the RSA signal is straightforwardly connected with the long-living hole spin polarization component $\Sigma_\mathrm{h}^{(\mathrm{long})}$, as other components vanish. In the previous sections, two mechanisms of creating $\Sigma_\mathrm{h}^{(\mathrm{long})}$ in the TRKR signal were discussed: precession- and decoherence-induced. The same mechanisms are responsible for the formation of the RSA signal. First, the resonant pumping case, with no fast initial

decoherence ($u = w = 0$), will be discussed. For zero magnetic field, the precession-induced mechanism does not work, so there is no long-living spin polarization in the system and, therefore, no RSA signal (see Fig. 4.9). Then, with increasing magnetic field, precession induced mechanism starts working and more and more spin-polarized holes survive recombination, leading to the increase of the RSA amplitude [of course there are still minima and maxima, corresponding to destructive and constructive interference, the structure of which is reflected in Eq. (4.24) by P and Q]. With a further increase of magnetic field, the RSA amplitude begins to decrease because of the hole ensemble dephasing due to the g-factor inhomogeneity (see Fig. 4.9).

When the fast hole spin decoherence takes place in the system (due to non-resonant or high-power pumping) the description changes. Now, for zero magnetic field, when precession-induced mechanism does not work, decoherence-induced one is present and creates long-living spin polarization oriented oppositely to the one created by the first mechanism (see Fig. 4.9). Then, with increasing magnetic field, the precession-induced mechanism becomes more efficient and competes with decoherence-induced one. At some point it becomes more efficient and the sign of RSA signal changes. This competition between the two mechanisms is reflected by the envelope factor f in Eq. (4.24). In the limiting cases for $u = 0$ or $\omega_\mathrm{t} = 0$ it is always negative or positive, respectively. The competition of these two mechanisms can also be seen by analysing the phase shift of the TRKR signal [see Eqs. (4.13), (4.14) and Fig. 4.6]. Since every maximum of the RSA signal comes from the constructive interference of the long-living polarizations created by subsequent pulses, its value (and particularly the sign) depends on the initial value of long-living spin polarization component $\Sigma_\mathrm{h}^{(\mathrm{long})}(0)$. Now, by changing the magnetic field and fast decoherence parameter, the phase shift α can move the inital values of $\Sigma_\mathrm{h}^{(\mathrm{long})}$ from negative values (black, cyan and green lines in Fig. 4.6 and corresponding red regions in Fig. 4.9) through 0 (blue line in Fig. 4.6 and the corresponding green points in Fig. 4.9) to positive values (pink and red lines in Fig. 4.6 and corresponding blue region in Fig. 4.9).

Two kinds of RSA experiments in Voigt geometry were performed by the Regensburg group: for different excitation wavelengths and different pumping powers. Detuning and power ranges were the same as in the case of Kerr signal measurements in the absence of magnetic field (up to 7 meV detuning, and power range varying up to three orders of magnitude). Experiments were performed at a nominal sample temperature of 1.2 K and the time delay between the pulses was set to 12.5 ns (corresponding to the laser repetition rate of 80 MHz). Eq. (4.24), after averaging over the Gaussian distribution of the hole g-factors, allows one to closely model the RSA signal shape and, with the use of least-square fit algorithm, to extract the values of various physical characteristics of the hole

spin system. Experimental RSA traces together with the fits and extracted parameters, for both detuning and power measurement series, are presented in Figs. 4.10 and 4.11, respectively.

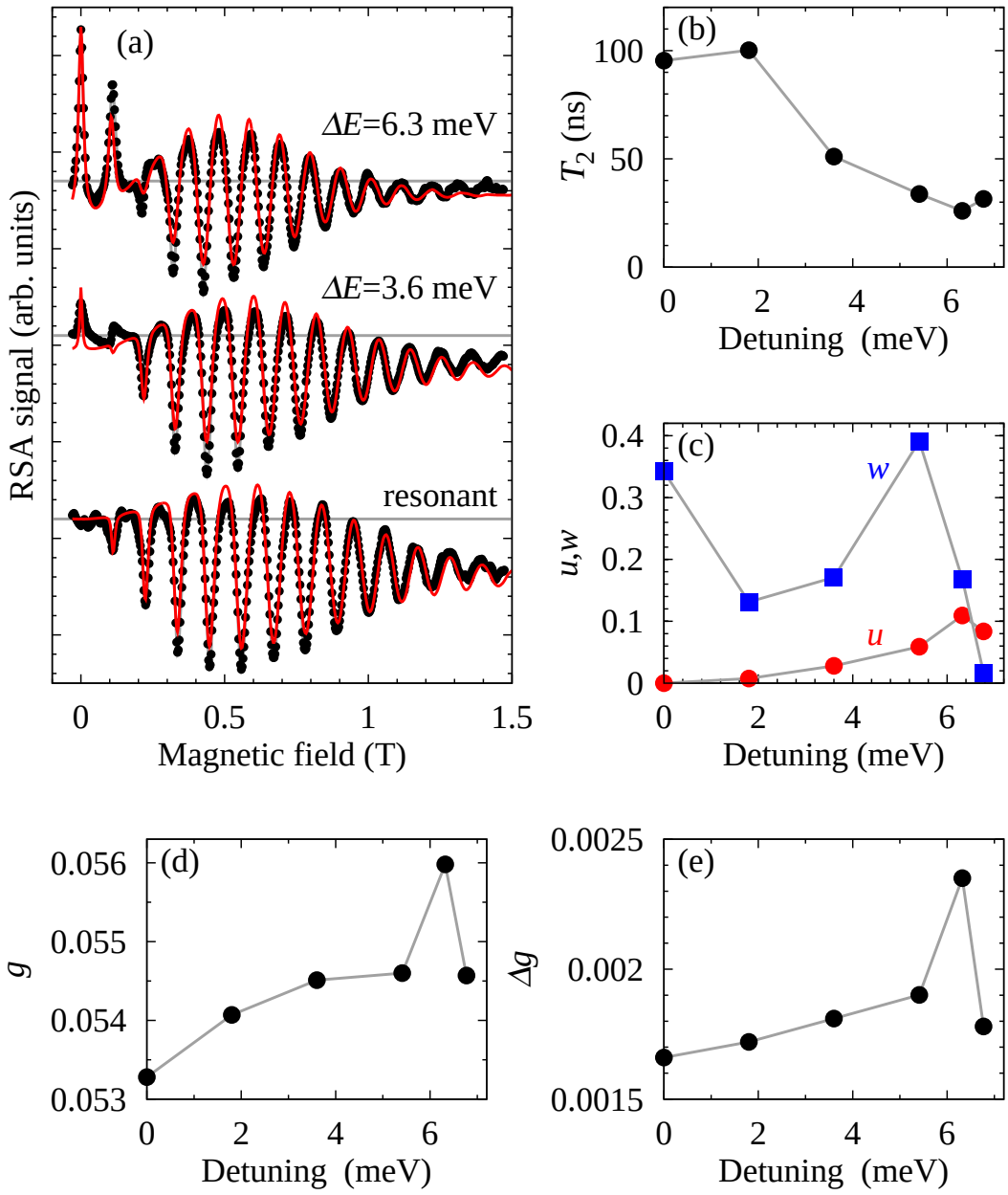

Figure 4.10: (a) Experimental RSA traces (black points) and best fits (red lines) for selected values of the detuning. (b)-(e) Parameter values extracted from the fitting: the dephasing time (b), the fast decoherence parameters (c), the hole g-factor (d), and the standard deviation of the g-factor distribution in the ensemble (e). Experimental data source: Ref. [15].

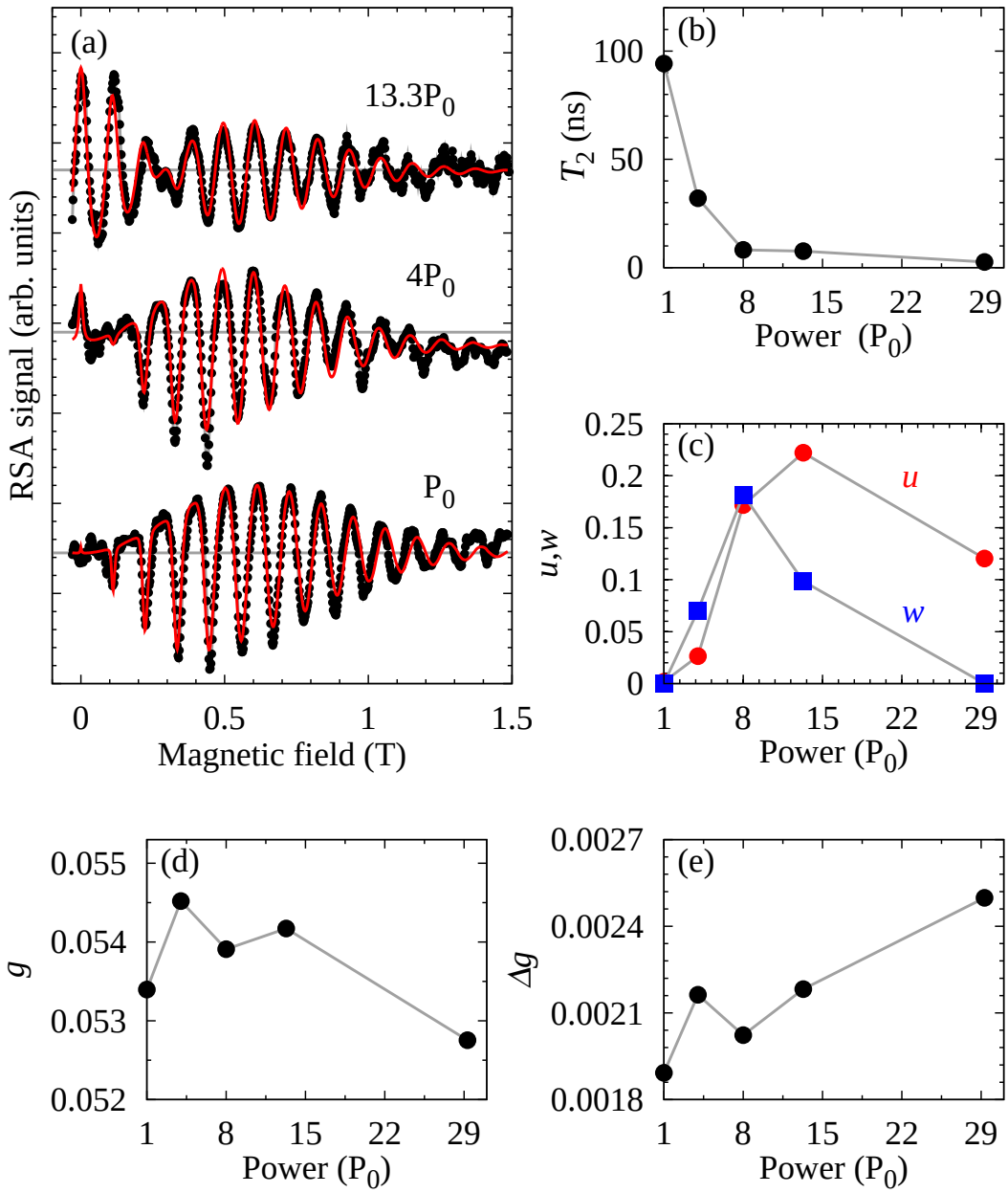

Figure 4.11: (a) Experimental RSA traces (black points) and best fits (red lines) for selected values of the excitation density. (b)-(e) Parameter values extracted from the fitting: the dephasing time (b), the fast decoherence parameters (c), the hole g-factor (d), and the standard deviation of the g-factor distribution in the ensemble (e). Experimental data source: Ref. [15].

For the off-resonant case, the value of the transverse spin dephasing time T_2 increases for decreasing detuning and saturates for low detunings at about 100 ns. The ratio of hole and trion spin polarization after fast initial decoherence, $\Sigma_{\mathrm{h}}(0)/\Sigma_{\mathrm{t}}(0) = -\exp(-u)$, reaches -1 as the resonance is approached. This shows that the off-resonant excitation at low temperatures leads only to a small loss of the optical orientation, which disappears

completely at resonance. The dephasing factor w, however, remains finite even at the resonance. This results from the fact, that spin dephasing is induced by an optical excitation due to selective coupling of the light field to one of the spin states (according to the selection rules) [19]. Both the hole g-factor and the standard deviation of the ensemble g-factor distribution tend to increase with the growing detuning. This may be explained by a reduced absorption of the pump pulse as the detuning is increased, which leads to a reduction of the sample temperature and a smaller spin-polarized hole ensemble. A shift of the hole g-factor to larger absolute values with temperature reduction has already been observed [3] and a smaller ensemble is more susceptible to g-factor inhomogeneity.

In the power series case, similar effects in the RSA traces are observed for increasing pump power at resonant excitation conditions. Here, the growing fast dephasing is due to the considerably increased amount of energy pumped into the system, which leads to an increased density of various excitations. This results in a stronger spin non-conserving scattering, before photocarrier recombination takes place, as observed in the TRKR measurements. The spin dephasing time T_2 also decreases with increasing pumping powers, most likely due to sample heating. This interpretation is supported by the fact that the hole g-factor slightly decreases with increasing pumping power, as expected for an increasing sample temperature.

Resonant excitation in different magnetic field configurations

The analytical formula for the RSA signal in tilted magnetic field is too complex, due to the dependecies on the angles θ and ϕ, to find its clear physical interpretation. Moreover, because of the complicated structure of the expression, it is hard to fit to the experimental data and extract the dynamical parameters of the system. Therefore, the only thing that was achieved is the reproduction of the general qualitative behaviour of the RSA signal shape. As can be seen in Fig. 4.12, for tilted fields, the RSA signal acquires the Gaussian-like envelope, centred at the zero magnetic field. This experimentally observed behaviour is reproduced by the model. However, due to lack of clear analytical formula, its origin has not been explained yet.

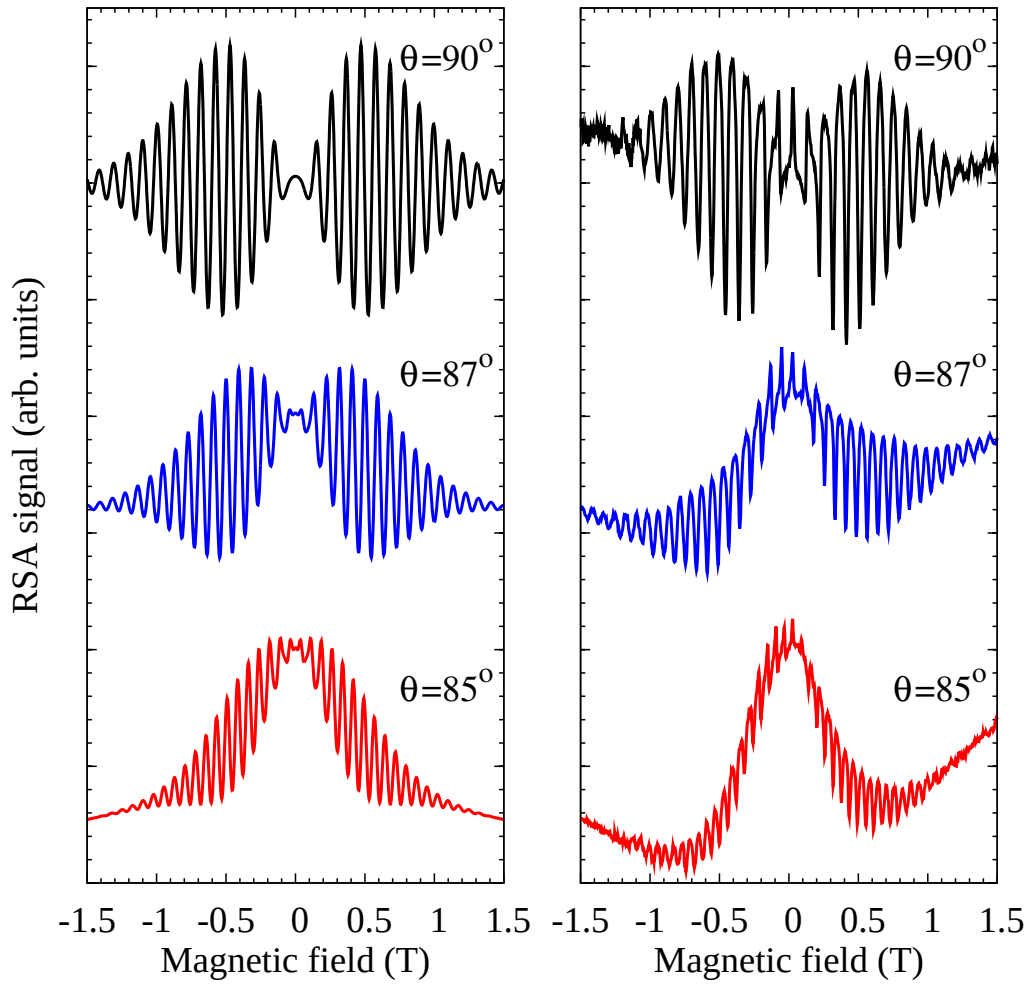

Figure 4.12: Experimental (right) and modeled (left) RSA traces for different angles θ (tilt angle $\alpha = 90^{\circ} - \theta$). Zero-field peaks in experimental signals are observed, due to non-resonant excitation, and are not connected with the tilt angle. Experimental data source: unpublished data by the courtesy of Tobias Korn and Michael Kugler.

4.3 Microscopic model of decoherence

Results related to the theory discussed in Chapter 3 will now be presented. In order to find the localized spin lifetime dependence on temperature, first Eq. (3.3) was numerically solved to find the chemical potential of the system for different temperatures, $\mu(T)$. The solution was found for the total carrier concentration $p = 1.1 \cdot 10^{11}$ cm^{-2} (which is the experimentally measured concentration in the sample used by the Regensburg group) and few values of $x > 1$, i.e. different proportions of the number of trapping centres to the total number of carriers in the system. During calculations, the energies of localization centres were assumed to be normally distributed around $E_0 = -1$ meV, with the standard

deviation $\sigma_E = 0.1$ meV. Then, with the use of calculated chemical potential, the distribution function for the free holes as a function of temperature, $n(T)$, was found [see Eq. (3.4)]. This way, the scattering probabilities between free and localized states could be calculated for different temperatures. However, in order to obtain numerical values, the localized state parameters had to be chosen. Using the estimates described in Chapter 3, the following values of the Gaussian widths of the localized state wavefunction, σ and σ_z, were found for 4 nm wide sample, investigated by the Regensburg group:

$$\sigma_z = 1.8\text{nm},$$

$$1.8\text{nm} < \sigma = 7.5\text{nm}.$$

As can be seen in Fig. 4.13, the localized spin lifetime τ (inverse of the scattering probability rate) is almost independent of the in-plane size of the localized state wavefunction in the estimated range of σ. However, as shown in Fig. 4.14, it strongly depends on the average number of trapping centres per carrier and increases with growing x. The calculated localized hole spin lifetimes are much smaller than the experimentally observed ones ($\sim$ 10 ns in 15 K and $\sim$ 100 ns in 1.2 K). This may be caused by three factors. First, which is the least probable, is that localization potentials are much deeper than 1 meV. Secondly, there may be much more localization centres than carriers, i.e. $x \gg 1$. It is, however, also quite unlikely, because, as can be seen in Fig. 4.14, the increase of x increases the lifetimes mostly at very low temperatures, and already around $T = 5$ K the differences in lifetimes for different values of x are very small. Finally, the inconsistency of the modeled results with experimental data may originate from the oversimplified model. As mentioned in Chapter 3, two mechanisms, which decrease the spin-flip probability, were omitted in the proposed approximated model. These are the reduction of the density of released holes in the vicinity of the localized carrier (induced by the Coulomb repulsion) and screening of the trapped hole.

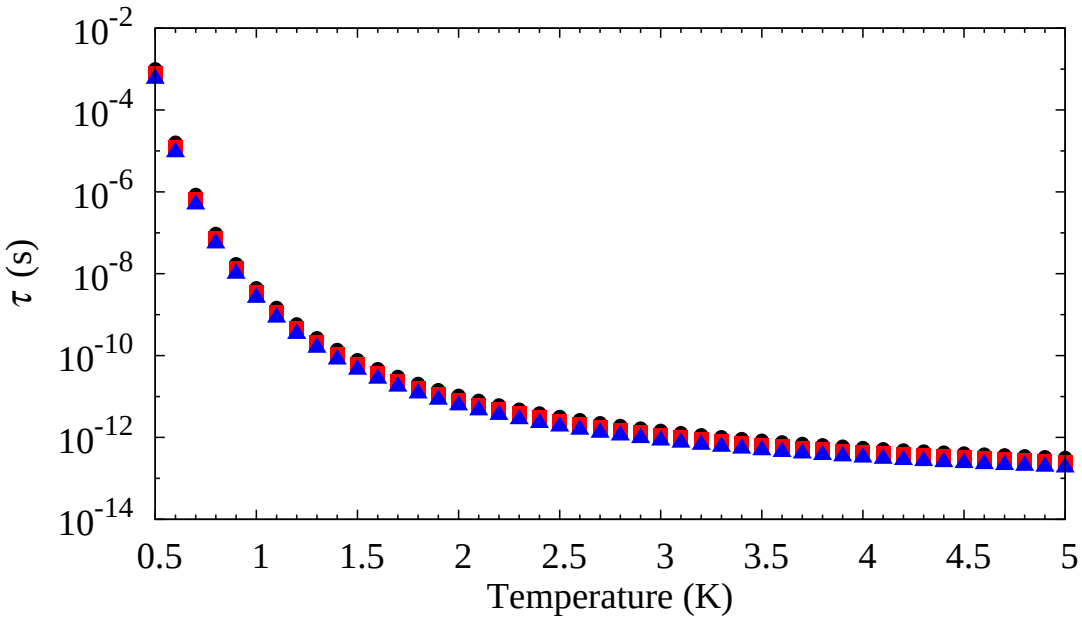

Figure 4.13: Temperature dependence of the calculated localized hole spin lifetime τ for $\sigma = 3$ nm (black circles), $\sigma = 5$ nm (red squares) and $\sigma = 7$ nm (blue triangles). Calculations performed for fixed $x = 5$.

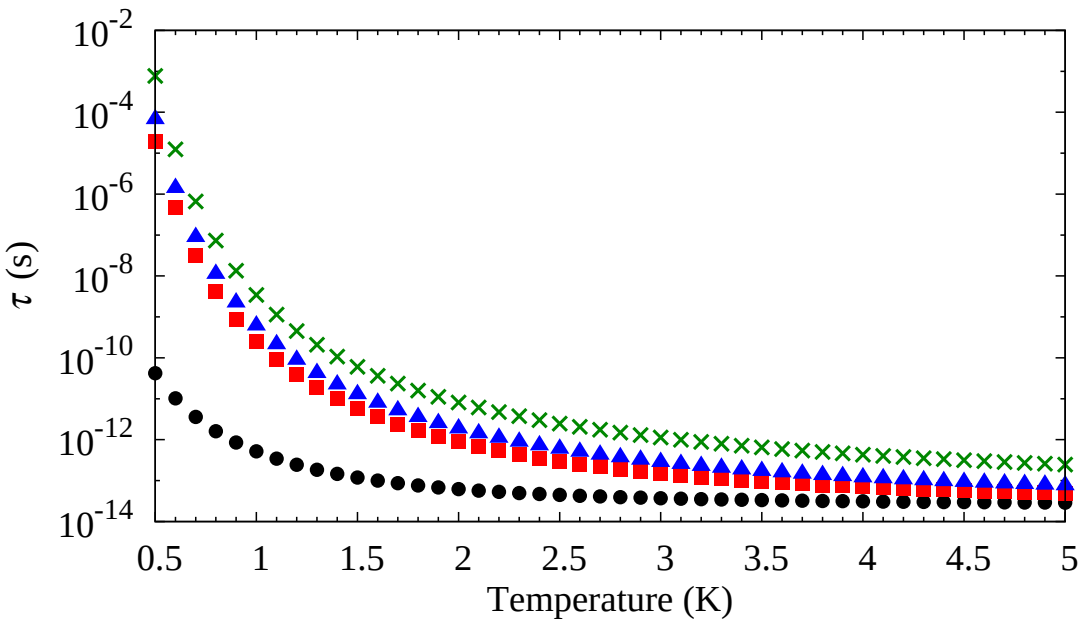

Figure 4.14: Temperature dependence of the calculated localized hole spin lifetime τ for $x = 1$ (black circles), $x = 1.5$ (red squares), $x = 2$ (blue triangles) and $x = 5$ (green Xs). Calculations performed for fixed $\sigma = 5$ nm.

Appendix: Mathematical formalism of open quantum systems

This appendix contains basic information about the notation and methods used in the theory of open quantum systems based on Ref. [20].

Density matrix

The Gleason's theorem states that if the dimension of Hilbert space $\mathcal{H}$ corresponding to the considered system is greater than 2, then the state of the system can be represented by linear operator acting on this Hilbert space: $\rho \in \mathcal{L}(\mathcal{H})$, with the following properties

$$\begin{array}{lll} 1. \ \langle A \rangle & = & \mathrm{Tr}(\rho A), \\ 2. \ \mathrm{Tr}\,\rho & = & 1, \\ 3. \ \rho & = & \rho^{\dagger}, \end{array}$$

where $\langle A \rangle$ is the average value of any observable A connected with the system.

For an open quantum system, i.e. the system (S), which is coupled to environment (E), the Hilbert space of the whole system is a tensorial product of the system and environment Hilbert spaces: $\mathcal{H}_{\mathrm{S+E}} = \mathcal{H}_{\mathrm{S}} \otimes \mathcal{H}_{\mathrm{E}}$. If one is now interested only in the properties of the system itself, i.e. the observables of the form $A \otimes \mathbb{I}$, the reduced density matrix can be introduced,

$$\rho_{\mathrm{S}} = \mathrm{Tr}_{\mathrm{E}}(\rho), \tag{A.1}$$

where $\rho = \rho_{\mathrm{S+E}}$ denotes the full density matrix of the system and environment and Tr_{E} is the trace over environmental degrees of freedom. Now, using the reduced density matrix, the average value of the observable A connected only with the system is given by

$$\langle A \rangle = \mathrm{Tr}(\rho_{\mathrm{S}} A).$$

Evolution of the density matrix

The evolution of the density matrix is given by the Liouville-von Neumann equation,

$$\dot{\rho}(t) = \frac{1}{i\hbar}[H(t), \rho(t)]. \tag{A.2}$$

Integrating this equation one obtains

$$\rho(t) = \frac{1}{i\hbar}\int_{t_0}^{t} d\tau [H(\tau), \rho(\tau)] + \rho(t_0). \tag{A.3}$$

Inserting Eq. (A.3) into Eq. (A.2) one arrives at the formal equation of motion for the density matrix,

$$\dot{\rho}(t) = \frac{1}{i\hbar}\left[H(t), \rho(t_0) + \frac{1}{i\hbar}\int_{t_0}^{t} d\tau [H(\tau), \rho(\tau)]\right]. \tag{A.4}$$

The next step is to decompose the Hamiltonian of the whole system H (which is assumed to be independent of time) into the free Hamiltonian part H_0 (corresponding to the evolution of the system S itself) and the interaction part H_{int} (corresponding to to the interaction of the system S with the environment E): $H = H_0 + H_{\text{int}}$. Now, for the time-independent H_0, one may use the unitary transformation and transform the density matrix and interaction part of the Hamiltonian into the interaction picture,

$$\begin{aligned} \tilde{\rho}(t) &= e^{iH_0 t/\hbar}\rho(t)e^{-iH_0 t/\hbar}, \\ \tilde{H}_{\text{int}} = H_{\text{int}}(t) &= e^{iH_0 t/\hbar}H_{\text{int}}e^{-iH_0 t/\hbar}, \end{aligned}$$

where $\tilde{\rho}(t)$ and $H_{\text{int}}(t)$ denote the density matrix and interaction part of Hamiltonian in the interaction picture. Density matrix $\tilde{\rho}(t)$ also satisfies the (modified) Liouville-von Neumann equation,

$$\dot{\tilde{\rho}}(t) = \frac{1}{i\hbar}[H_{\text{int}}(t), \tilde{\rho}(t)].$$

Finally, using the already obtained results for the reduced density matrix [Eq. (A.1)] and the formal equation of motion for the density matrix [Eq. (A.4)], one arrives at the equation of motion of the reduced density matrix in the interaction picture (which is still exact),

$$\dot{\tilde{\rho}}_{\text{S}}(t) = -\frac{i}{\hbar}\,\text{Tr}_{\text{E}}[H_{\text{int}}(t), \tilde{\rho}(t_0)] - \frac{1}{\hbar^2}\,\text{Tr}_{\text{E}}\int_{t_0}^{t} d\tau\,[H_{\text{int}}(t), [H_{\text{int}}(\tau), \tilde{\rho}(\tau)]]\,. \tag{A.5}$$

Approximations

The first assumption is that there exist two timescales: $\tau_{\text{env}} \ll \tau_{\text{S}}$, where τ_{env} is the characteristic time of the environment relaxation and τ_{S} is the characteristic time of the

system evolution. Due to the relatively fast relaxation of the environment one can assume that it is in thermal equilibrium all the time,

$$\tilde{\rho}(t) = \tilde{\rho}_{\mathrm{S}}(t) \otimes \tilde{\rho}_{\mathrm{E}},$$

with the time independent equilibrium density matrix of the environment given by

$$\tilde{\rho}_{\mathrm{E}} = \rho_{\mathrm{E}} = \rho^{(\mathrm{eq})} = \frac{1}{Q_N} e^{-\beta H_E},$$

with Q_N and β being the statistical sum and inverse temperature ($1/k_{\mathrm{B}}T$) respectively. Of course, in this assumption the assumption of separable state at initial time (no correlations) is included, $\tilde{\rho}(t_0) = \tilde{\rho}_{\mathrm{S}}(t_0) \otimes \rho^{(\mathrm{eq})}$.

Next, one can show that the first term in Eq. (A.5), i.e. $\mathrm{Tr}_{\mathrm{E}}[V(t), \tilde{\rho}(t_0)]$, is responsible only for the rescaling of the energy in the system, so it can be neglected (because it does not affect the interaction).

Before going further, the interaction term $H_{\mathrm{int}}(t)$ is rewritten in the explicit form of the product of operators acting on the system and environment,

$$\begin{aligned} H_{\mathrm{int}}(t) &= \sum_{ij} \sigma_{ij}(t) \otimes R_{ij}(t), \\ \sigma_{ij}(t) &= e^{i(E_i - E_j)t/\hbar} |i\rangle\langle j| = e^{-i\omega_{ij}t} |i\rangle\langle j|, \\ R_{ij}(t) &= e^{iH_{\mathrm{E}}t/\hbar} R_{ij} e^{-iH_{\mathrm{E}}t/\hbar}, \end{aligned} \tag{A.6}$$

where $|i\rangle$, $|j\rangle$ are the eigenstates of the system Hamiltonian, $H_{\mathrm{S}}|i\rangle = E_i|i\rangle$, and R_{ij} are corresponding environment operators. Now the equation of motion of the reduced density matrix in the interaction picture can be written in the form

$$\dot{\tilde{\rho}}_{\mathrm{S}}(t) = -\frac{1}{\hbar^2} \sum_{ijkl} \int_{t_0}^{t} d\tau \left[\sigma_{ij}(t)\sigma_{kl}(\tau)\tilde{\rho}_{\mathrm{S}}(\tau) - \sigma_{kl}(\tau)\tilde{\rho}_{\mathrm{S}}(\tau)\sigma_{ij}(t)\right] R_{ijkl}(t-\tau) + \mathrm{h.c.}$$

where $R_{ijkl}(t-\tau) = \langle R_{ij}(t) R_{kl}(\tau)\rangle = \langle R_{ij}(t-\tau) R_{kl}\rangle$ are the correlation functions of the environmental operators, which act as the memory functions with characteristic time τ_{mem} (which means that for arguments much greater than τ_{mem} the memory functions vanish). After changing the integration variable $t - \tau \to s$,

$$\begin{aligned} \dot{\tilde{\rho}}_{\mathrm{S}}(t) &= -\frac{1}{\hbar^2} \sum_{ijkl} \int_{0}^{t-t_0} ds \left[\sigma_{ij}(t)\sigma_{kl}(t-s)\tilde{\rho}_{\mathrm{S}}(t-s)\right. \\ &\quad \left. -\sigma_{kl}(t-s)\tilde{\rho}_{\mathrm{S}}(t-s)\sigma_{ij}(t)\right] R_{ijkl}(s) + \mathrm{H.c.}, \end{aligned} \tag{A.7}$$

one more approximation is made. Namely, the assumption is made that the considered times are much bigger than the memory time: $t - t_0 \gg \tau_{\mathrm{mem}}$. This results in invalidity of the equation for the very short timescales (comparable with τ_{mem}), but allows one to

extend the upper limit of integration to infinity, $t - t_0 \to \infty$, since for big arguments the memory function vanishes and this extension does not affect the result. Finally, taking into account that $\tilde{\rho}_{\rm S}$ changes slowly during $\tau_{\rm mem}$ one can put $\tilde{\rho}_{\rm S}(t-s) = \tilde{\rho}_{\rm S}(t)$. This way one arrives at the Markovian equation

$$\dot{\tilde{\rho}}_{\rm S}(t) = -\frac{1}{\hbar^2}\sum_{ijkl}\int_0^\infty ds\,[\sigma_{ij}(t)\sigma_{kl}(t-s)\tilde{\rho}_{\rm S}(t) - \sigma_{kl}(t-s)\tilde{\rho}_{\rm S}(t)\sigma_{ij}(t)]\,R_{ijkl}(s) + \text{H.c.} \quad \text{(A.8)}$$

Spectral densities

Spectral densities are definied as the Fourier transforms of correlation functions,

$$R_{ijkl}(\omega) = \frac{1}{2\pi\hbar^2}\int_{-\infty}^{\infty} ds e^{i\omega s} R_{ijkl}(s), \quad \text{(A.9)}$$

$$R_{ijkl}(s) = \hbar^2 \int_{-\infty}^{\infty} d\omega e^{-i\omega s} R_{ijkl}(\omega). \quad \text{(A.10)}$$

Spectral densities have the properties

$$\begin{aligned} 1.\quad R_{ijkl}(-\omega) &= e^{-\hbar\omega/k_{\rm B}T} R_{klij}(\omega), \\ 2.\quad R_{ijkl}(\omega) &= R_{klij}(-\omega), \\ 3.\quad R^*_{ijkl}(\omega) &= R_{lkji}(\omega). \end{aligned}$$

With the use of spectral densities and system operators σ_{ij} [definied in Eq. (A.6)] the Markovian equation of motion for the reduced density matrix in the interaction picture, Eq. (A.8), can be written in the form

$$\begin{aligned} \dot{\tilde{\rho}}_{\rm S}(t) &= -\pi\sum_{ijkl}\left[\sigma_{ij}\sigma_{kl}\tilde{\rho}_{\rm S}(t) - \sigma_{kl}\tilde{\rho}_{\rm S}(t)\sigma_{ij})e^{-i(\omega_{ij}+\omega_{kl})t}R_{ijkl}(\omega_{kl})\right] \quad \text{(A.11)} \\ &\quad + i\sum_{ijkl}\mathcal{P}\int_{-\infty}^{\infty} d\omega\left[\sigma_{ij}\sigma_{kl}\tilde{\rho}_{\rm S}(t) - \sigma_{kl}\tilde{\rho}_{\rm S}(t)\sigma_{ij})e^{-i(\omega_{ij}+\omega_{kl})t}\frac{R_{ijkl}(\omega)}{\omega-\omega_{kl}}\right] + \text{H.c.} \end{aligned}$$

The second part of this equation (together with its hermitian conjugate) has the form $[h, \tilde{\rho}_{\rm S}(t)]$, where h is a hermitian operator. Therefore this part of the evolution equation is non-dissipative and is responsible for shifting of the energy levels. Because the main focus is put here on the dissipative influence of the environment on the system dynamics the non-dissipative part will be neglected.

The remaining first part of Eq. (A.11) (together with its hermitian conjugate) can be transformed back to the Schrödinger picture in order to obtain the evolution equation of the form

$$\dot{\rho}_{\rm S}(t) = -\frac{i}{\hbar}[H_0, \rho_{\rm S}(t)] + \mathcal{L}[\rho_{\rm S}(t)], \quad \text{(A.12)}$$

with the Lindblad superoperator $\mathcal{L}[\rho_{\rm S}(t)]$, responsible for dissipative dynamics, given by

$$\begin{aligned} \mathcal{L}[\rho_{\rm S}(t)] &= -\pi\sum_{ijkl}\left[(\sigma_{ij}\sigma_{kl}\rho_{\rm S}(t) - \sigma_{kl}\rho_{\rm S}(t)\sigma_{ij})R_{ijkl}(\omega_{kl})\right. \\ &\quad \left. + (\rho_{\rm S}(t)\sigma_{ij}\sigma_{kl} - \sigma_{kl}\rho_{\rm S}(t)\sigma_{ij})R_{ijkl}(-\omega_{ij})\right]. \quad \text{(A.13)} \end{aligned}$$

Bibliography

[1] J. Fabian, A. Matos-Abiague, C. Ertler, P. Stano, and I. Žutić, Acta Physica Slovaca **57**, 565 (2007).

[2] M. W. Wu., J. H. Jiang, and M. Q. Weng, Physics Reports **493**, 61 (2010).

[3] M. Syperek, D. R. Yakovlev, A. Greilich, J. Misiewicz, M. Bayer, D. Reuter, and A. D. Wieck, Phys. Rev. Lett. **99**, 187401 (2007).

[4] J. J. Baumberg, D. D. Awschalom, N. Samarth, H. Luo, and J. K. Furdyna, Phys. Rev. Lett. **72**, 717 (1994).

[5] J. M. Kikkawa and D. D. Awschalom, Phys. Rev. Lett. **80**, 4313 (1998).

[6] M. Syperek, D. R. Yakovlev, I. A. Yugova, J. Misiewicz, I. V. Sedova, S. V. Sorokin, A. A. Toropov, S. V. Ivanov, and M. Bayer, Phys. Rev. B **84**, 085304 (2011); **84**, 159903(E) (2011).

[7] D. J. Hilton and C. L. Tang, Phys. Rev. Lett. **89**, 146601 (2002).

[8] K. Shen and M. W. Wu, Phys. Rev. B **82**, 115205 (2010).

[9] T. Korn, M. Kugler, M. Griesbeck, R. Schulz, A. Wagner, M. Hirmer, C. Gerl, D. Schuh, W. Wegscheider, and C. Schüller, New J. Phys. **12**, 043003 (2010).

[10] T. Korn, Phys. Rep. **494**, 415 (2010).

[11] J. R. Petta, A. C. Johnson, J. M. Taylor, E. A. Laird, A. Yacoby, M. D. Lukin, C. M. Marcus, M. P. Hanson, and A. C. Gossard, Science **309**, 2180 (2005).

[12] R. Winkler, S. J. Papadakis, E. P. De Poortere, and M. Shayegan, Phys. Rev. Lett. **85**, 4574 (2000).

[13] T. Andlauer and P. Vogl, Phys. Rev. B **79**, 045307 (2009).

[14] M. Kugler, T. Andlauer, T. Korn, A. Wagner, S. Fehringer, R. Schulz, M. Kubová, C. Gerl, D. Schuh, W. Wegscheider, P. Vogl, and C. Schüller, Phys. Rev. B **80**, 035325 (2009).

[15] M. Kugler, K. Korzekwa, P. Machnikowski, C. Gradl, S. Furthmeier, M. Griesbeck, M. Hirmer, D. Schuh, W. Wegscheider, T. Kuhn, C. Schüller, and T. Korn, Phys. Rev. B **84**, 085327 (2011).

[16] P. Machnikowski and T. Kuhn, Phys. Rev. B **81**, 115306 (2010).

[17] I. A. Yugova, M. M. Glazov, E. L. Ivchenko, and A. L. Efros, Phys. Rev. B **80**, 104436 (2009).

[18] M. I. D'yakonov and V. I. Perel', Sov. Phys. Solid State **13**, 3023-3026 (1971).

[19] A. Grodecka, P. Machnikowski, and J. Förstner, Phys. Rev. A **79**, 042331 (2009).

[20] H.-P. Breuer and F. Petruccione, *The Theory of Open Quantum Systems* (Oxford University Press, Oxford, 2002).